

FUEL EFFICIENT GALAXIES: SUSTAINING STAR FORMATION WITH STELLAR MASS LOSS

SAMUEL N. LEITNER AND ANDREY V. KRAVTSOV

Department of Astronomy & Astrophysics, The University of Chicago, Chicago, IL 60637 USA and
Kavli Institute for Cosmological Physics and Enrico Fermi Institute, The University of Chicago, Chicago, IL 60637 USA
Draft version October 31, 2018

ABSTRACT

We examine the importance of secular stellar mass loss for fueling ongoing star formation in disk galaxies during the late stages of their evolution. For a galaxy of a given stellar mass, we calculate the total mass loss rate of its entire stellar population using star formation histories derived from the observed evolution of the M_* -star formation rate relation, along with the predictions of standard stellar evolution models for stellar mass loss for a variety of initial stellar mass functions. Our model shows that recycled gas from stellar mass loss can provide most or all of the fuel required to sustain the current level of star formation in late type galaxies. Stellar mass loss can therefore remove the tension between the low gas infall rates that are derived from observations and the relatively rapid star formation occurring in disk galaxies. For galaxies where cold gas infall rates have been estimated, we demonstrate explicitly that stellar mass loss can account for most of the deficit between their star formation and infall rates.

Subject headings: cosmology: theory – galaxies: evolution – galaxies: formation – stars:formation – methods: numerical

1. INTRODUCTION

An understanding of how galaxies get their gas is key to a complete picture of galaxy formation and evolution. At all redshifts, star forming galaxies appear to be living fast and dangerously: they are observed to be converting their gas to stars at a rapid rate that would lead to exhaustion of their cold gas reservoirs in about two billion years without a fresh supply of gas (Kennicutt 1998; Leroy et al. 2008; Bigiel et al. 2008; Genzel et al. 2010; Daddi et al. 2010b,a). Observations, however, also show that star forming galaxies are common at all redshifts, and theoretical models indicate that star formation rates of the most actively star forming systems are set by their cold gas accretion rates (e.g., Davé et al. 2010; Bouché et al. 2010). In addition, since the average neutral hydrogen density in the universe has dropped by only 50% over 10 billion years in the face of much higher gas consumption rates, the cold gas supply must be getting continuously replenished (e.g., Bauermeister et al. 2010; Prochaska & Wolfe 2009; Putman et al. 2009a).

Despite its importance, the mechanism by which gas is replenished in nearby galaxies is a major puzzle (see, e.g., Sancisi et al. 2008; Putman et al. 2009a, for reviews). Clouds of neutral hydrogen are observed around the Milky Way, M31 and a number of other nearby galaxies (e.g., Blitz et al. 1999; Wakker et al. 2007; Miller et al. 2009; Thilker et al. 2004), but both the fate of these clouds and the fraction of their gas that they deposit in their host’s disks are uncertain. Direct searches in nearby groups of galaxies have failed to uncover massive populations of clouds of neutral hydrogen (Pisano et al. 2007). Nevertheless, estimates for the accretion rate due to high velocity HI clouds (HVCs) have been made for a handful of galaxies, and typical values range from 10% to 20% of the current SFR of the parent galaxy (see Sancisi et al. 2008, for a review, and table 2 below).

The accretion of gas rich satellite galaxies provides a second potential source of fresh gas for massive star forming host galaxies (e.g., Sancisi et al. 2008). Larger satellites have the potential to carry fresh gas to the star forming disk of their hosts when they merge, and such a scenario is likely

in the case of M31 and M33 for example (Putman et al. 2009c). However, due to the gas stripping that occurs during the most common minor mergers, satellites will tend to deposit their gas at large radii, well beyond the radius of their host’s star forming disk (Peek 2009; Grcevich & Putman 2009). Sancisi et al. (2008) estimate that some nearby galaxies accrete gas from satellites at a rate of $\sim 10 - 20\%$ of the SFR of their hosts, although this number could be significantly lower on average (Kauffmann et al. 2010).

Such low gas accretion rates could imply that galaxies are presently in the stage of exhausting their gas reservoirs and ceasing star formation activity. However, this would leave questions about the gas supply during the past several billion years, because the evolution of the disk galaxy population is inconsistent with a complete shutdown of star formation (e.g., Bauermeister et al. 2010; Bell et al. 2007).

So far, predictions of theoretical models as to how gas is delivered to galaxy disks are quite uncertain. While theoretical studies predict broadly that the average accretion rate of baryonic mass onto dark matter halos should be several times their SFRs today (e.g., Dekel et al. 2009, eq 1), the timescale and route by which the baryonic mass reaches galaxy disks themselves is difficult to predict (e.g., Faucher-Giguere et al. 2011). Most of the baryons accreted at low redshifts are thought to encounter previously accreted material and suffer shocks, instabilities, and fragmentation (e.g., Kereš & Hernquist 2009); these events may mix the accreting gas with hot halo gas before it has a chance to reach the star forming disk where it is needed. Although such hot gas may cool at the disk-halo interface and contribute to star formation at a later time, this gas may not be immediately available.

Given that a large gas reservoir may surround galaxy disks, an inviting solution to the gas deficit problem is to tap this hot gas through mixing with colder gas on hot phase/cold phase boundaries. This mixing would elevate the cooling rate of the hot coronal gas, and allow it to sink onto the galaxy, thereby producing net accretion. Such mixing could occur in the galactic fountain (e.g., Marinacci et al. 2010; Fraternali & Binney 2008) and, intriguingly, might explain

the decrease in angular momentum that is observed in gas with increasing height above the Milky Way disk. Mixing has also been proposed to cool gas out of the halo at the interface between the hot halo and dwarf satellites (Bland-Hawthorn 2009). Unfortunately, the predictions of these models are rather uncertain because magnetic fields, conduction and poorly constrained gas density, and temperature, can all have leading-order effects on the final mass of gas that cools during mixing (e.g., Marinacci et al. 2010; Heitsch & Putman 2009). Even without physical uncertainties, the resolution required to track the detailed cooling of the halo gas may be beyond what is achievable by current simulations (e.g., an ability to resolve the cooling layer may be necessary), so the thermodynamics and fate of the accreting gas are both difficult to model and are poorly constrained.

Before exploring unconstrained and difficult to model mechanisms for accretion, all other channels should be fully understood. A significant internal gas channel – the stellar population itself – has not been rigorously explored in this context. Stellar populations can shed a significant fraction ($\sim 30 - 50\%$) of their mass over the Hubble time through secular processes, particularly via shedding of the stellar envelopes during the Asymptotic Giant Branch (AGB) phase (e.g., Vassiliadis & Wood 1993; Hurley et al. 2000; Groenewegen et al. 2007). In comparison, the Milky Way requires only $\sim 2\%$ of its stellar mass to be returned to ISM per billion years to balance its gas consumption by star formation. Stellar mass loss should be an accessible fuel for star formation in disk galaxies because winds are typically injected directly into the relatively dense interstellar medium (ISM) with cool temperatures $< 3 \times 10^3 K$, low velocities $\sim 10 \text{ km s}^{-1}$ and largely in molecular form (e.g. Knapp 1990; Marengo 2009; Libert et al. 2010, and references therein).

Mass return by stellar populations is noted in the seminal study of (Roberts 1963), which was the first to discuss the transience of galaxy populations as a result of gas consumption. Sandage (1986) and Kennicutt et al. (1994) both made the important observation that recycled material could extend gas consumption timescales in the nearby disk galaxy population. More recently, Blitz (1997) has pointed to observations demonstrating that the mass of gas lost in the Milky Way could be a significant source of fuel. Nevertheless, in recent literature, stellar mass loss is generally not considered as part of the gas supply budget outside of some chemical enrichment studies.

Many codes for simulating galaxy formation have only recently begun to incorporate stellar mass loss (Katz et al. 1996; Kravtsov & Gnedin 2005; Stinson et al. 2006) and recent studies indicate that it can be an important physical ingredient, significantly influencing galaxy morphologies (Agertz et al. 2010; Martig & Bournaud 2010) and providing substantial fuel source for continuing star formation at $z = 0$ (Schaye et al. 2010).

The goal of this study is to carefully assess the potential importance of stellar mass loss in fueling star formation of late-type galaxies at low redshifts ($z < 1$), by making use of observational constraints from star formation measurements. To this end, we estimate the total loss rates averaged over entire galaxies for empirically motivated star formation histories (SFHs) and show that stellar mass loss could be an important source of fresh gas for star formation at late epochs. In particular, we explicitly demonstrate that gas returned to the ISM by stars can provide most of the gas required to maintain current level of star formation in a number of nearby galaxies, for

which the observed accretion rate of halo gas clouds appears to be insufficient to fully resupply the gas reservoir.

To estimate the global stellar mass loss rate for a galaxy we need a mass loss model that describes the mass loss rate of a single age stellar population as a function of time and a star formation history describing the age distribution of all stellar populations in a galaxy. Mass loss modeling and its uncertainties are discussed in § 2. We calculate star formation histories in § 3 based on empirical measurements of the slope and evolution of the relation between stellar mass and the star formation rate of star forming disk galaxies. The resulting global stellar mass loss rates that our model predicts are presented in § 4, where we also derive mass loss rates for several nearby galaxies that are then compared to the observed difference between star formation and cold gas infall. Our results and conclusions are discussed in § 5. Finally, the Appendix explores the extent to which recycled material might accumulate over time based on the results of cosmological galaxy formation simulations and simple models that reproduce those simulations.

2. MODELING MASS LOSS

To first order, the mass recycled by a single-age stellar population (SSP) comes from mass that is lost by stars that have evolved through the luminous, wind-driving, SNe, red supergiant and/or asymptotic giant branch stages, minus the total mass in compact stellar remnants. The fraction of mass lost by a SSP population at a given time t after its birth is therefore approximately the fraction of the population’s stellar mass that was initially possessed by stars with masses above the main sequence turn off $m \geq m_{\text{to}}$, minus the fraction of mass that remains locked in the remnants from those same stars (see e.g., Kalirai et al. 2008, for empirical constraints on the remnant mass fraction). Here we will use mass loss rates tabulated from stellar evolution tracks to estimate the amount of mass lost by an SSP, but calculating mass loss from a main sequence turnoff time (Raiteri et al. 1996) and the initial-final mass relation (from Kalirai et al. 2008) as in Agertz et al. (2010), results in only small differences (5–10% less mass loss in the first 2 Gyr) from what is presented below.

The underlying IMF sets the fraction of stars with mass above $m_{\text{to}}(t)$. A number of commonly used IMFs are parameterized in table 1, where we define ξ to be the number of stars per logarithmic mass interval. These parameterizations include broken power laws for different mass intervals,

$$\xi(\ln(m)) \propto m^{-\Gamma}$$

and lognormal distributions,

$$\xi(\ln(m)) \propto \exp \left[\frac{-(\log_{10}(m) - \log_{10}(m_c))^2}{2\sigma^2} \right].$$

Corresponding cumulative stellar fractions for different IMFs are plotted in the left panel of Figure 1, which shows that systematic differences between IMFs at $1M_{\odot}$, which corresponds to the main-sequence turnoff mass after the 10 Gyr, are $\approx 20\%$. At larger masses, corresponding to younger population ages, the differences can be as large as a factor of $\approx 2 - 3$.

The right hand panel of figure 1 shows cumulative stellar mass loss as a function of time for SSPs with the same IMFs and of solar metallicity. These were calculated in FSPS (Conroy & Gunn 2010) using the Padova stellar evolu-

tion models¹ (based on Marigo et al. 2008; Marigo & Girardi 2007; Girardi et al. 2000)

The figure shows that the majority of stellar mass loss occurs in the first two billion years, but there is a persistent slow rate of mass loss continuing to late times. The differences in mass loss for different IMFs after several billion years can be as large as a factor of two. However, for the range of IMFs considered to be likely for stellar populations in normal galaxies (see, e.g., Kroupa 2007) the differences are $\lesssim 30\%$.

The fraction of mass lost for each case is well fit by the functional form of Jungwiert et al. (2001). Namely, the cumulative fraction of mass lost by a stellar particle at a time t since its birth is given by

$$f_{\text{ml}}(t) = C_0 \ln\left(\frac{t}{\lambda} + 1\right) \quad (1)$$

fit parameters C_0 and λ are given in table 1.

Although the rates of mass loss in any particular phase of stellar evolution may be metal dependent and mass loss rate measurements for individual stars in that phase may exhibit factor of $\lesssim 4$ scatter (e.g., Maun & Josselin 2010), the important quantity here is the observed initial-final mass relation. This appears to be a weak function of metallicity, such that a $Z = 0.1Z_{\odot}$ population will lock approximately the same amount of mass in remnants as a solar metallicity population (e.g., Kalirai et al. 2008, Marigo & Girardi 2007). Uncertainty in the IMF is therefore the dominant source of uncertainty in estimating the amount of mass loss from a SSP.

To represent the plausible range of IMFs (see recent review by Bastian et al. 2010, for an extensive discussion of observational constraints on the possible range of IMFs), we adopt the commonly used Chabrier (2003, hereafter C03) IMF and its steep version, stpC03. The latter has the same log-normal form as the C03 IMF below $1M_{\odot}$, but a slope that is steeper than Salpeter (1955) by 0.35 above $1M_{\odot}$. These choices bracket the range of IMFs that are favored by observations²: they include the observed flattening of the mass function at low masses (Miller & Scalo 1979; Kroupa et al. 1993), and also encompass the range of high mass slopes that are allowed by observations, when theoretical uncertainties in unresolved binary stars (Kroupa et al. 1991; Kroupa 2007), dynamical evolution in clusters and other effects are considered (Kroupa & Weidner 2003; Bastian et al. 2010). Although they are listed in our tables and shown for comparison, we choose not to bracket the low mass loss case with either the original power law Salpeter (1955) IMF or the Scalo (1986) IMF because both are thought to predict too many low mass stars ($< 1M_{\odot}$ Miller & Scalo 1979; Kroupa et al. 1993; Scalo 1998; Chabrier 2001), and over predict dynamical mass (Bell & de Jong 2001; Cappellari et al. 2006). Unless otherwise noted, C03 will be used as the fiducial IMF in this study.

3. THE STAR FORMATION AND MASS LOSS HISTORIES OF GALAXIES

With mass loss rates for SSPs in hand, the age distribution of stellar populations that are losing mass, i.e. star formation histories, are needed to determine the relevance of the galaxy-wide mass loss to the gas budget and for fueling continuing star formation at low z .

¹ <http://stev.oapd.inaf.it/cgi-bin/cmd>

² The C03 and stpC03 cumulative mass functions vary by no more than 5% from the Kroupa (2001) and Kroupa et al. (1993) mass functions respectively, meaning their mass loss rates are very similar.

To this end, we will use a model of SFHs derived from the observed relation between SFR and stellar masses of galaxies at different redshifts. The SFHs can be derived in this way because stellar mass in disk galaxies is primarily the integral of the in-situ SFR modulo mass loss. Given the observed evolution of the SFR- M_* relation with redshift for actively star forming galaxies, SFHs for galaxies of a given current stellar mass, $M_{*,0}$, can be derived by starting with $M_{*,0}$, integrating the stellar mass back in time and determining the corresponding SFR at each epoch z using the evolving $M_*(z)$ and the SFR- M_* relation at that epoch. Such a procedure is justified because scatter in the SFR- M_* relation is relatively small: the distribution of SFR(M_*) at a given z is approximately log-normal with a $1\sigma_*$ of ≈ 0.3 dex (Noeske et al. 2007). This implies that the galaxy population spends $\approx 95\%$ of its time, and builds up $\approx 87\%$ of its stellar mass, during periods when SFRs are within a factor of four ($< 2\sigma_*$) of the median at a given epoch. Nevertheless, we explore the effect of the scatter in the SFR- M_* relation on mass loss rates more thoroughly in § 3.3. A more detailed discussion of average star formation histories derived from measures of instantaneous star formation rate will be presented in a separate paper (Leitner 2011, in preparation). Although SFHs of individual galaxies might be determined more accurately by fitting population synthesis models to galaxy spectra, the approach we adopt here should provide an average estimate of the importance of stellar mass loss for galaxies of a given stellar mass.

Implicit in this strategy for deriving SFHs is the assumption that mergers play no significant role in stellar build-up and that a galaxy's stellar mass changes solely because it forms stars or loses mass through stellar mass loss. Mergers have the potential to split M_* as lookback time increases, thereby slightly increasing the SFR for the ensemble of progenitors compared to the values derived using our model. If mergers were an important factor in the growth of low- z galaxy stellar mass, the SFR derived using our model would be underestimated resulting in galaxies forming more of their stellar mass at shorter lookback time. There is evidence, however, that the effect of mergers on the buildup of stellar mass is not large for most disk galaxies of $M_{*,0} \lesssim 10^{11}M_{\odot}$ at low redshifts. For example, both Bell et al. (2007, see Figure 4) and Drory & Alvarez (2008) show that a scheme similar to ours reproduces the buildup of the stellar mass function of all galaxies with only a minor contribution from mergers. Furthermore, Conroy & Wechsler (2009) derive average SFHs for galaxies using the subhalo abundance matching method and show that mergers of galaxy halos cannot play a significant role in the evolution of the stellar mass function of galaxies at $z < 2$.

3.1. The Observed Evolution of the SFR- M_* Relation

A number of studies have explored the evolution and shape of the SFR- M_* relation at complementary UV and infrared wavelengths (Noeske et al. 2007; Elbaz et al. 2007; Salim et al. 2007; Daddi et al. 2007, 2009; Stark et al. 2009; González et al. 2010, see the compilation of results by Dutton et al. 2010). Recently, Oliver et al. (2010) performed a far-infrared stacking survey at 70 and 160 μm , and included 100 μm and 160 μm observations from the Herschel satellite (Rodighiero et al. 2010), which allowed them to probe regions of the SED less affected by uncertainties in dust absorption. Oliver et al. (2010) derived a fit to the median evolution and shape of the SFR- M_* relation of star forming galaxies in their sample. The redshift evolution they derive is plot-

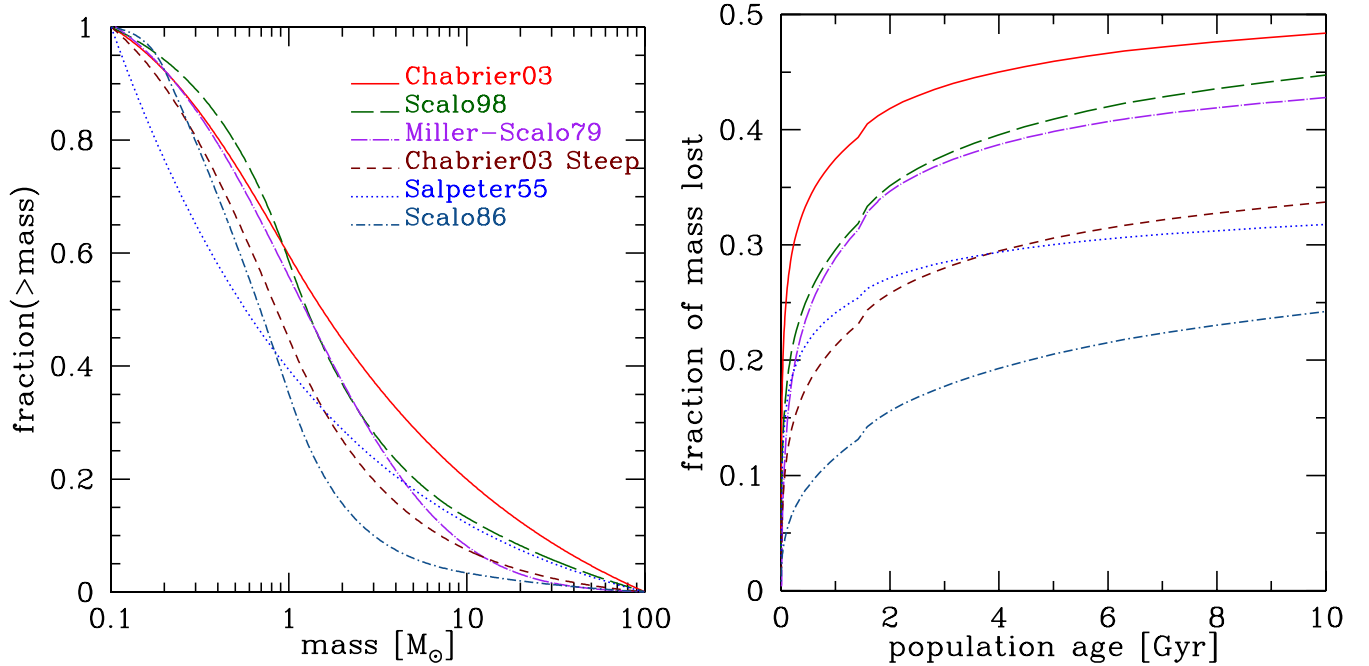


Figure 1. *Left panel:* The fraction of stellar mass in stars of mass $> m$ for a number of commonly used IMFs. *Right panel:* The fraction of mass lost as a function of age for a single-age stellar population. Chabrier03 and Chabrier03 Steep were chosen to bracket the effect of likely IMF choices on mass loss rates in our study (see text for details).

Table 1
Mass loss and the IMF

IMF	Functional form	Mass loss fits	
		C_0	λ [yr]
Chabrier (2003) [C03] (similar to Kroupa 2001)	$m < 1M_{\odot}$: log-normal ($\sigma = 0.69, m_c = 0.08$) $m > 1M_{\odot}$: power-law ($\Gamma = 1.3$)	0.046	2.76×10^5
Steep Chabrier (2003) [stpC03] (similar to Kroupa et al. 1993)	$m < 1M_{\odot}$: log-normal ($\sigma = 0.69, m_c = 0.08$) $m > 1M_{\odot}$: power-law ($\Gamma = 1.7$)	0.051	1.33×10^7
Scalo (1998) [S98]	$m < 1M_{\odot}$: $\Gamma_1 = 0.2$ $1M_{\odot} < m < 10M_{\odot}$: $\Gamma_2 = 1.7$ $m > 10M_{\odot}$: $\Gamma_3 = 1.3$	0.062	6.97×10^6
Miller & Scalo (1979)	log-normal ($\sigma = 0.74, m_c = 0.95$)	0.058	6.04×10^6
Salpeter (1955)	$\Gamma = 1.35$	0.032	5.13×10^5
Scalo (1986) ^a	$m < 0.2$: $\Gamma_1 = -2.6$; $0.2 < m < 1M_{\odot}$: $\Gamma_2 = 0.80$ $1M_{\odot} < m < 10M_{\odot}$: $\Gamma_3 = 2.25$ $m > 10M_{\odot}$: $\Gamma_4 = 1.45$	0.055	1.25×10^8

^aA fit from Mo et al. (2010) with an extension to $m < 0.2$.

ted as a solid line along with the points from previous studies in Figure 2. The figure shows a general consistency between different observations at $z \lesssim 1$ (points have been scaled to $M_* = 10^{10.75} M_{\odot}$ according to the SFR- M_* relation provided for each separate data set in Dutton et al. 2010). Studies including quiescent galaxies (e.g., Zheng et al. 2007) also match the recent IR-derived results (Oliver et al. 2010), indicating that systematic errors are under control (although see Rodighiero et al. 2010, for recent L_{IR} -SFR calibration from Herschel). In this study, we use the fit of Oliver et al. (2010)

at $z < 2$.

At $z > 1$ uncertainty in the normalization and slope of the SFR- M_* relation increases and there is a possibility that an evolving IMF may affect the evolution (Davé 2008; Wilkins et al. 2008, but see Bastian et al. 2010). Fortunately, the build-up of stellar mass at $z > 2$ does not significantly affect estimates of stellar mass loss at $z = 0$ for late type galaxies, which are the focus of our study. Furthermore, late-type galaxies with $M_* < 10^{11} M_{\odot}$ appear to build up most of their stellar mass at $z \lesssim 1$, so the evolution of star formation rates at

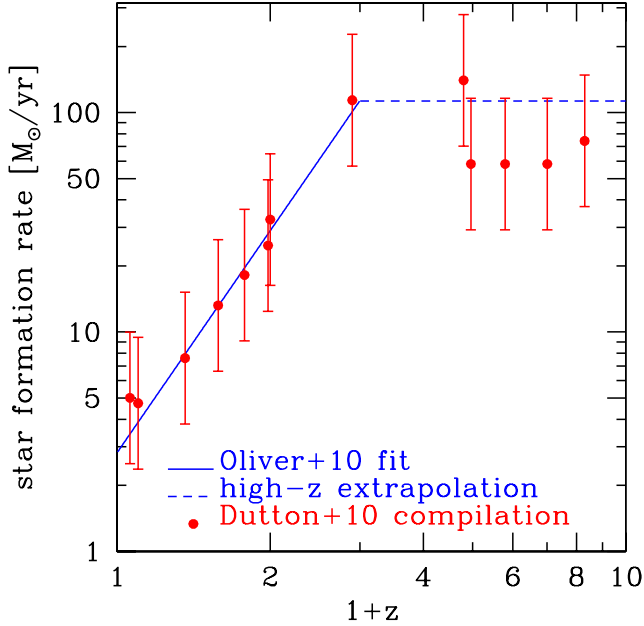


Figure 2. Observations of the evolution of the normalization of the SFR- M_* relation at the stellar mass $M_* = 10^{10.75} M_\odot$ with redshift for various data sets. The red points are from the Dutton et al. (2010) compilation of data from González et al. (2010); Stark et al. (2009); Daddi et al. (2009, 2007); Elbaz et al. (2007); Noeske et al. (2007); Salim et al. (2007). The error bars show the estimated factor of two scatter of galaxies about $\psi(M_*, z)$. At $z \lesssim 2$, the blue line is the fit to the far infrared data of late-type star forming galaxies from Oliver et al. (2010), which shows good agreement with previous studies. At $z > 2$, we assume that normalization of the SFR- M_* is constant (dashed line).

high redshifts is not very important (see figure 3). We mimic the high redshift evolution with a redshift independent SFR that forms a broken power law with $z_{\text{break}} = 2$.

Recent measurements of the slope β in the relation $\text{SFR} \propto M_*^{\beta+1}$ at fixed epoch, show $-0.5 < \beta < 0$ at $z < 1$. Whether β remains constant with redshift (Zheng et al. 2007), evolves to a shallower value (e.g., Brinchmann et al. 2004; Noeske et al. 2007; Elbaz et al. 2007), or steepens (Rodighiero et al. 2010; Erb et al. 2006; Oliver et al. 2010), is unclear at present. Here we assume a constant model with $\beta = -0.25$. The resulting global scaling we use for $z < z_{\text{break}}$ is,

$$\psi(M_*, z) = A_0 (z + 1)^\alpha \left(\frac{M_*}{10^{10.75} M_\odot} \right)^{1+\beta}, \quad (2)$$

where we adopt the power law slope of $\alpha \approx 3.4$ for late-type galaxies of $M_{*0} = 10^{10.75} M_\odot$ (Oliver et al. 2010). We label this fit to the median instantaneous SFR measurements ψ to distinguish it from the SFR that a specific galaxy experiences as a function of redshift (its SFH). The normalization A_0 to $\psi(M_*, z)$ (plotted in figure 2 for $M_* = 10^{11} M_\odot$) is $2.8 M_\odot \text{yr}^{-1}$ (Oliver et al. 2010). Uncertainty in α and β will be discussed further in section 3.2.

For $z_{\text{break}} < z < 6$ we use $\alpha = 0$, and assume that all initial stars in a galaxy form in a burst at $z = 6$ (these stars constitute only a few percent of M_{*0}).

3.2. Calculating Star Formation and Mass Loss Histories

The overall global mass loss rate (GMLR) of a galaxy is equal to its SFR convolved with the fractional mass loss rate \dot{f}_{ml} (whose integral is given by eq. 1):

$$\text{GMLR}(t) = \int_{t_0}^t \text{SFR}(t') \dot{f}_{\text{ml}}(t - t') dt' \quad (3)$$

In our toy model, the evolution of the stellar mass of a galaxy is given by,

$$\dot{M}_*(t) = \psi(M_*, z) - \text{GMLR}(t) \quad (4)$$

with boundary condition $M_*(t = 0) = M_{*0}$, where $\psi(M_*, t)$ is the instantaneous SFR function from eq. 2, which is a function of the *evolving* mass of the galaxy M_* . The SFH of the galaxy is then given by,

$$\text{SFR}(t) = \psi(M_*(t), z) \quad (5)$$

The GMLR(t) term introduces a complication in that it is defined as a convolution of the SFR of a galaxy with its fractional mass loss rate up to time t , but the SFH of the galaxy is not, at first, known. As a first guess, we can take $\text{GMLR}(t) = 0$, derive $M_*(t)$, plug the resulting SFH into eq. 2 and iterate to convergence,

$$\begin{aligned} \dot{M}_*^{(0)}(t) &= \psi(M_*^{(0)}, t) \\ \text{SFR}^{(0)}(t) &= \psi(M_*^{(0)}(t), z) \\ \dot{M}_*^{(1)}(t) &= \psi(M_*^{(1)}, t) - \text{GMLR}(\text{SFH}^{(0)}, t) \\ \text{SFR}^{(1)}(t) &= \psi(M_*^{(1)}(t), z) \\ &\vdots \end{aligned} \quad (6)$$

Star formation and stellar mass loss histories are plotted in Figure 3 for several representative values of M_{*0} and the fixed median SFR scaling relation discussed in § 3.1.

In the right panel of Figure 3, we show the effect of the uncertainty in the parameters α ($\sigma_\alpha \approx \pm 0.5$) and β ($\sigma_\beta \approx \pm 0.25$) on the SFH and the mass loss rates (based on estimates by Oliver et al. 2010, and dispersion in the literature discussed above). The observational 1σ uncertainty in the slope and evolution of the SFR- M_* relation only translates into uncertainty in the mass loss rate of $< 5\%$ at $z = 0$, although the differences can be relevant to the stellar mass loss history.

3.3. The Impact of Scatter in the SFR- M_* Relation

Although the observed scatter in the SFR- M_* relation is relatively small, deviations from the median relation can be significant for some galaxies and may thus affect conclusions about the importance of stellar mass loss. In this section, we will therefore consider the effects of populating the scatter in SFR- M_* relation, with a range of possible SFH scenarios. We parameterize the scatter around the star formation rate function $\psi(M_*, z)$ that an individual galaxy experiences, with the time scale, τ_Δ , over which deviations around the median relation occur, and by the magnitude of scatter, σ_* . We assume that the scatter is described by a log-normal function with the median described by the relation in equation 2. We thus multiply $\psi(M_*, z)$ at a given redshift by $N(t, \tau_\Delta, \sigma_*)$ – a log-normal random number sampled every τ_Δ for $t > \tau_\Delta$. To force the model to trend toward the assigned $\text{SFR}(z = 0)$, we set $N(t, \tau_\Delta, \sigma_*) = \text{SFR}(z = 0)/A_0$ for lookback times $< \tau_\Delta$.

The effect of scatter is illustrated in Figure 4, which shows relative global stellar mass loss rates as a function of assumed

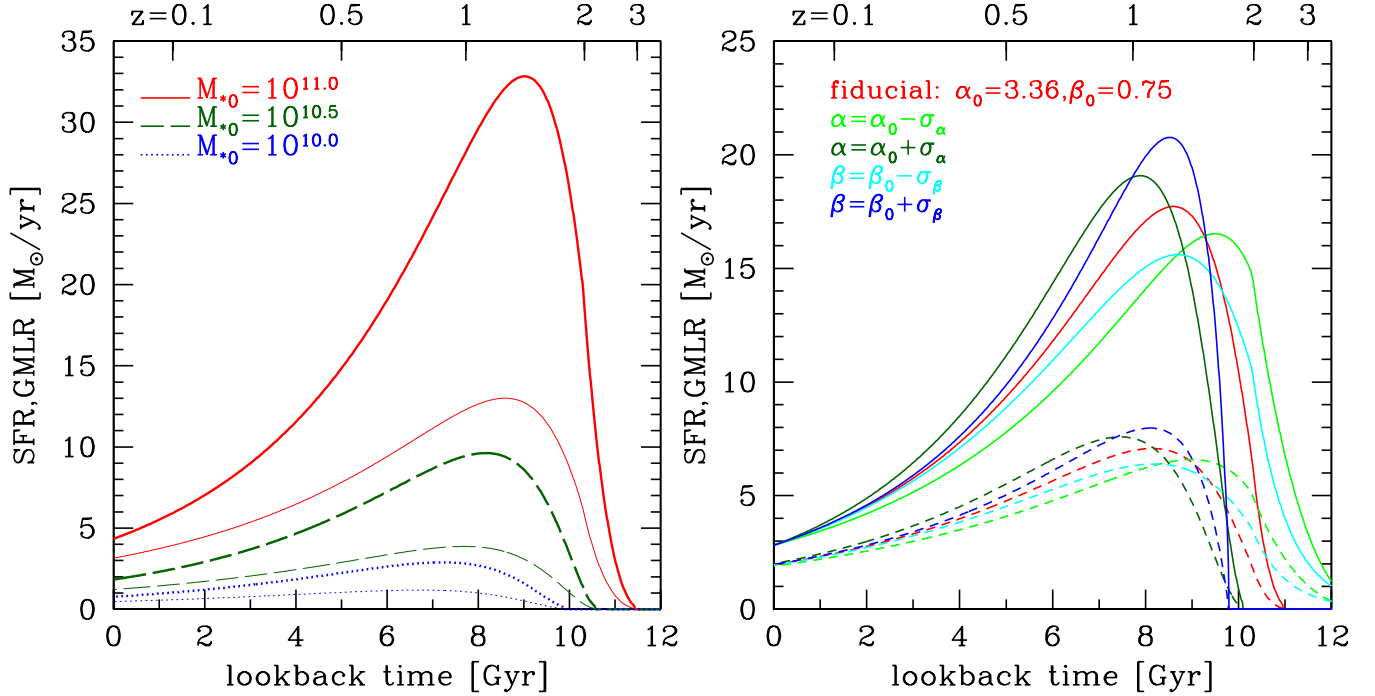


Figure 3. *Left Panel:* SFHs (*thick lines*) for galaxies of different $z = 0$ stellar mass, M_{*0} : $10^{11.0} M_{\odot}$ (red solid line), $10^{10.5} M_{\odot}$ (green dashed line), and $10^{10.0} M_{\odot}$ (blue dotted line). SFHs here are derived from the observed $\psi(M_*, z)$ (see § 3.2 for details). The *thin lines* of the corresponding color and line type show the global stellar mass loss rates for these SFHs. *Right Panel:* SFHs (*solid lines*) and stellar mass loss rates (*dashed lines*) calculated for a galaxy of $z = 0$ stellar mass of $M_{*0} = 10^{10.75} M_{\odot}$ with the values of parameters of $\psi(M_*, z)$, α and β (see eq. 2) varied by 1σ ($\sigma_{\alpha} \approx 0.5$ and $\sigma_{\beta} \approx 0.25$) from their average measured values (lines of different color, with color correspondence indicated in the legend). Note that stellar mass loss rate at low z is insensitive to 1σ variation of the parameters of $\psi(M_*, z)$ at this level.

τ_{Δ} for model galaxies with $M_* = 10^{10.75} M_{\odot}$ (the stellar mass of the Milky Way) and $\text{SFR}(z = 0)$ corresponding to the median SFR at that mass, as well as star formation rates at $\pm 1\sigma_*$ from the median. Mass loss rates are normalized by the population-average rate in the $\tau_{\Delta} = 0$ case. The overall amplitude of each line in the vertical direction therefore indicates the factor by which the mass loss rate is biased with respect to the case wherein galaxies, at any instant, draw their SFR randomly from the lognormal population-wide probability distribution function of SFRs. The shaded regions covers the area between the 16% and 84% outliers from the median mass loss rate at a given $\{\text{SFR}(z = 0), \tau_{\Delta}\}$.

The shaded region in the figure shows that that scatter in the $\text{SFR}-M_*$ relation results in small scatter in the mass loss rate for a given galaxy. The different present day SFRs also result in an overall change of the mass loss rate, although this effect disappears for very short τ_{Δ} .

Galaxy-wide stochasticity would presumably have a catalyst, such as a merger, tidal interaction, or rapid increase in gas accretion rate. These processes should operate on the crossing time of the halo (~ 1 Gyr) so we adopt $\tau_{\Delta} = 500$ Myr as a fiducial minimum value. We do not enforce a maximum τ_{Δ} , thus we use $\tau_{\Delta} = 14$ Gyr for the scenario in which the scatter around the median relation for the disk population is not generated by stochasticity in individual galaxies, but is instead caused by persistent environmental effects; these effects would be different for different galaxies in the population, but similar over time for a given galaxy. In other words, in such a scenario, a galaxy that has a SFR below $\psi(M_*)$ at some high

redshift will maintain a low SFR with respect to $\psi(M_*, z)$ at all z . The overall uncertainty in the global mass loss rates for a given mass loss model, encompassing both model dependence and the $\pm 1\sigma_{\Delta}$ outliers from stochastic variation with $\tau_{\Delta} = 500$ Myr, can then be quantified as the GMLRs encompassing these two regions. This uncertainty is marked by the black vertical dotted lines for each $\text{SFR}(z = 0)$ in Figure 4, and this method will be used to describe model uncertainty in the results below.

The star formation and stellar mass loss histories for model galaxies with $\tau_{\Delta} = 14$ Gyr are plotted in the right panel of Figure 4 for the same representative range of present day SFRs. The lower $\text{SFR}(z = 0)$ case results in less star formation at late times, and hence more star formation at high redshifts, as the total stellar mass is kept constant. This push-back also results in less stellar mass loss at low z , since a population loses more of its mass when it is younger. However, the decrease in mass loss rate is not proportional to the decrease in $\text{SFR}(z = 0)$, as is assumed by the instantaneous *recycling* approximation. This is because old populations continue to shed mass. In fact, the mass loss and star formation lines are very close to each other for the low $\text{SFR}(z = 0)$ case in Figure 4, indicating that stellar mass loss could be responsible for fueling almost all of the star formation in such a galaxy. Conversely, in galaxies with a higher current SFR for a given stellar mass loss provides a smaller fraction of the fuel required to maintain the star formation at the same level.

4. IMPLICATIONS OF STELLAR MASS LOSS FOR THE GAS SUPPLY IN GALAXIES

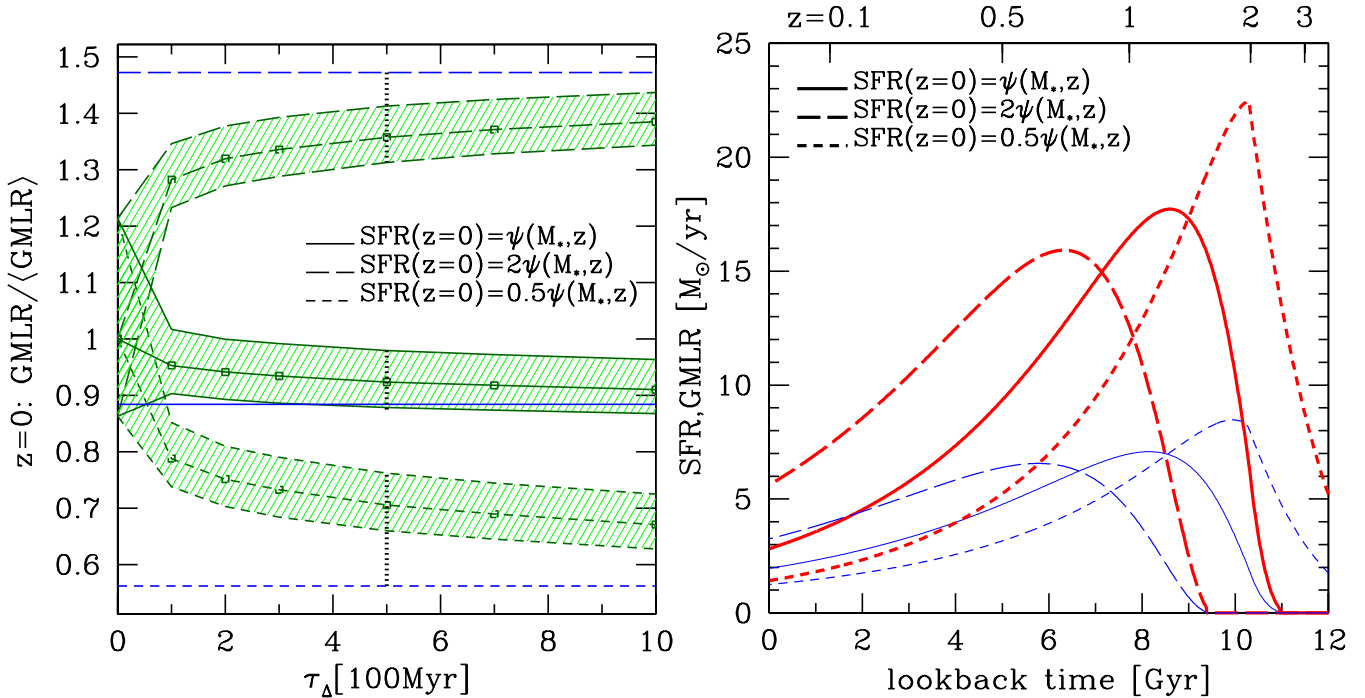


Figure 4. *Left Panel:* The $z = 0$ stellar mass loss rate for galaxies of $M_{*0} = 10^{10.75} M_\odot$ as a function of τ_Δ normalized to the population’s average mass loss rate in a scenario where galaxies draw their SFR randomly from a lognormal distribution about $\psi(M_*, z)$ at all times (i.e., $\tau_\Delta = 0$, see text for details). Solid, short dashed, and long dashed lines correspond to galaxies with present day SFR that are at the median (A_0), 16th ($0.5A_0$) and 84th ($2A_0$) percentile in the scatter about $\psi(M_*, z)$ at $M_{*0} = 10^{10.75} M_\odot$. Green regions encompass the 1σ scatter for a population about their corresponding relative mass loss rate, while blue lines show the $\tau_\Delta = 14$ Gyr limit for each present day SFR. The $\tau_\Delta = 14$ Gyr cases are systematically lower for each present day star SFR because the mean of a lognormal distribution is offset from the median. We take $\tau_\Delta > 500$ Myr so the difference between the mass loss rate with $\tau_\Delta = 500$ Myr and 14 Gyr, noted with vertical black dotted lines, marks the uncertainty in the mass loss model. *Right Panel:* Star formation (thick red) and stellar mass loss (thin blue) histories at $M_{*0} = 10^{10.75} M_\odot$ for $\tau_\Delta = 14$ Gyr. Line styles are the same as on the left. The model shows that stellar mass loss can provide a larger fraction of the fuel required to maintain star formation in galaxies with low $\text{SFR}(z = 0)$. In all cases, the global stellar mass loss rate is a significant fraction of the present day SFR.

4.1. $z = 0$ Stellar Mass Loss

Present day stellar mass loss rates for galaxies, calculated assuming both C03 and stpC03 IMFs (see § 2) are plotted in Figure 5 as a function of galaxy stellar mass. The additional infall that is required to match the consumption of gas by star formation is the difference between the SFR and stellar mass loss; it is shown by the hatched bands. The width of the shaded regions corresponds to uncertainty about the C03 and stpC03 IMFs caused by stochasticity (with $\tau_\Delta > 500$ Myr) that can comprise the scatter in the SFR- M_* relation, as discussed in § 3.3. Note that this uncertainty is relatively small and does not affect our conclusions about the importance of stellar mass loss.

The middle panel of Figure 5 shows that stellar mass loss dominates over infall across the entire plotted stellar mass range. For a stpC03 IMF, stellar mass loss still makes up a significant portion of the star formation but, on average, infall should comprise 45 – 60% of the star formation rate.

The side panels of Figure 5 show the amount of stellar mass loss for galaxies with present day star formation rates $\pm 1\sigma_*$ (i.e., a factor of two) away from the median SFR- M_* relation. The left panel shows that for galaxies with SFR below the median, stellar mass loss dominates over infall for both C03 and stpC03 IMFs. The right panel shows that galaxies with SFR higher than average require more significant infall to maintain their SFR. For the stpC03 IMF infall should contribute about

60% of the gas to maintain current SFR, whereas for the C03 IMF, stellar mass loss still dominates, but infall must make up for about 40 – 50% of the gas required to maintain the SFR.

4.2. Recycling Epoch

The epoch at which the stellar mass loss rate becomes larger than half of star formation rate is plotted in Figure 6. This period can be thought of as the *recycling epoch*, when stellar mass loss provides most of the new gas needed to replenish what is consumed by star formation. The figure shows that the recycling epoch occurs at $z \approx 0.7 - 0.9$, $z \approx 0.3 - 0.6$ and $\approx 0.05 - 0.2$ for the galaxies with respectively systematically low, median, and high star formation rates relative to $\psi(M_*, z)$. The recycling epoch is sensitive to the assumed IMF; for example, assuming stpC03 IMF instead of C03, galaxies that follow $\psi(M_*, z)$ enter the recycling epoch at $z \approx 0.1$.

4.3. The Gas and Star Formation Budget of Nearby Galaxies

It is only possible to estimate the cold gas accretion rate for a handful of galaxies. Nevertheless, available estimates are all considerably smaller than the current star formation rates of host galaxies, a fact that has been used to raise concerns of a sizable gas deficit (Fraternali 2010, 2009; Sancisi et al. 2008; Fraternali & Binney 2008; Putman et al. 2009b; Marinacci et al. 2010). It is thus interesting to evaluate the potential contribution of stellar mass loss.

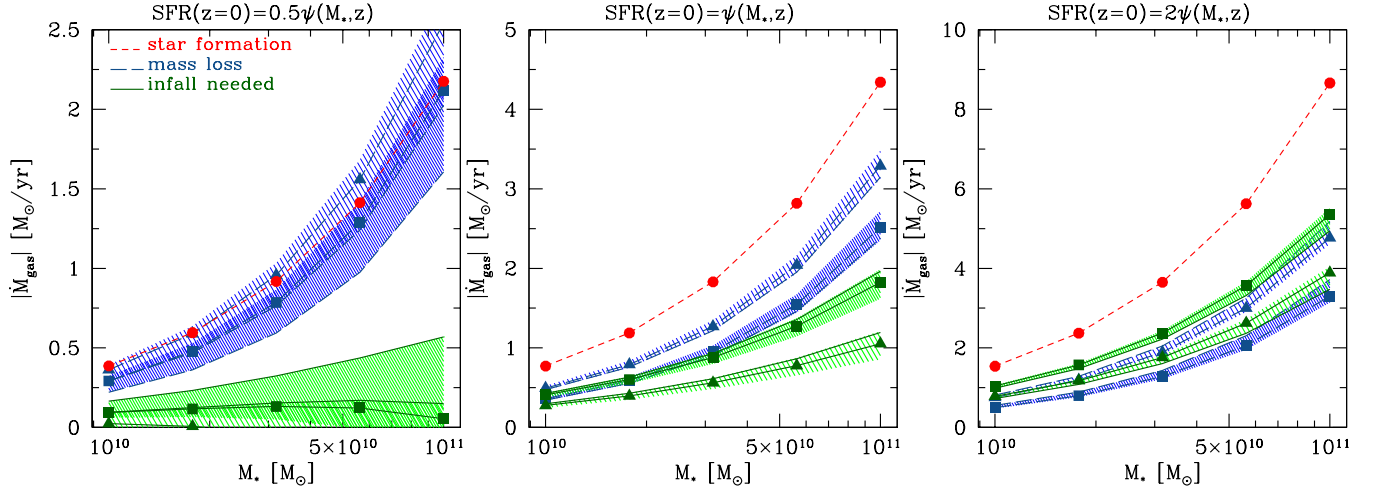


Figure 5. Average star formation rate (red dashed lines) and global stellar mass loss rate (blue dashed lines) as a function of stellar mass. The green solid lines show the difference between SFR and stellar mass loss rate. Lines without points are calculated assuming no stochastic scatter (i.e., $\tau_{\Delta} = 14$ Gyr), and lines with points are for the models with scatter assuming $\tau_{\Delta} = 500$ Myr timescale with a C03 (triangles), and stpC03 (squares) IMFs. Shaded regions represent modeling uncertainty for the C03 (lightly shaded) and stpC03 (densely shaded) IMFs, which includes plausible range of stochasticity in the SFR- M_* relation. The central panel is for median present day star formers, while the left and right panels are for galaxies with star formation rates higher and lower than the median by $1\sigma_*$, respectively. Note that in all panels stellar mass loss rate is a significant fraction of the SFR and is comparable to the SFR in the left panel (i.e., low SFR case).

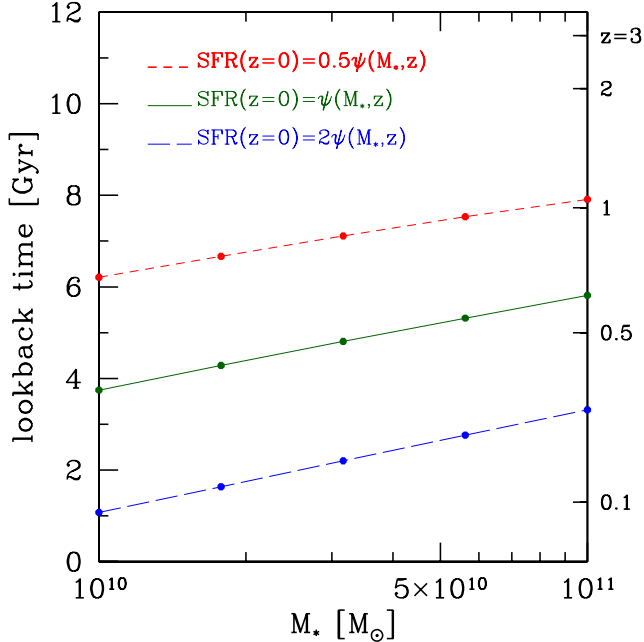


Figure 6. The lookback time at which the global stellar mass loss rates become larger than half the star formation rate, assuming a C03 IMF. The short (long) dashed line show such time for galaxies in the 16th (84th) percentile in SFR($z = 0$), while the solid lines show results for the median SFR- M_* relation.

The gas budgets for the galaxies with available estimates of gas infall rates are presented in Table 2 and Figure 7, including the expected contribution from stellar mass loss. To estimate the mass loss rate we use observational constraints on SFR($z = 0$) and M_{*0} as input and calculate present day stellar mass loss rates through modeled SFHs, as described above. For galaxies with a range of SFR($z = 0$) quoted in

the table, we use the high value to calculate the mass loss rates. This choice is conservative, because mass loss will make up a smaller fraction of the gas supply in galaxies with higher SFR at fixed stellar mass, as was shown above (see, e.g., Fig. 4 right panel). Ranges quoted for global stellar mass loss rates incorporate the scatter and modelling uncertainty that was quantified in § 3.3.

The table and figure show that total gas supply rates (stellar mass loss + gas infall) are close to star formation rates. Conservatively, the factor of several discrepancy between star formation and cold-HI gas supply (e.g., Fraternali 2009) should reduce to a factor of two discrepancy for some galaxies, and to zero or a surplus in others.

Furthermore, a less conservative accounting of infall may include factor of two or larger corrections to infall rates from (1) a 33% correction for the helium fraction, and (2) the fact that neutral gas only accounts for a fraction of the infalling cloud mass. The neutral fraction in the HVC clouds is not very well constrained at present with observational estimates ranging from $\sim 10 - 20\%$ for HVCs that are distant (Maloney & Putman 2003) to $\sim 50\%$ for the clouds near the disk (Wakker et al. 2007; Hill et al. 2009). Despite the uncertainties, it is clear that ionized gas constitutes a non-negligible mass fraction of the halo clouds (Sembach et al. 2003) and so the accretion rate observed in HI can only be a lower limit. There could also be additional possible sources of fresh gas, such as infall from gas rich satellites ($0.1 - 0.2 M_{\odot} \text{ yr}^{-1}$) and accretion that is lost in confusion noise (esp. for NGC 891), as discussed by Sancisi et al. (2008). Observations of the Milky Way suggest that $0.2 M_{\odot} \text{ yr}^{-1}$ of additional infall may have been already been observed (Wakker et al. 2008).

Finally, we note that empirical estimates of stellar mass loss exist for some nearby dwarf galaxies, such as LMC, WLM, and IC 1613, in which complete samples of AGB stars can be constructed and mass loss for individual AGB stars determined from the IR observations (Jackson et al. 2007a,b; Matsuura et al. 2009; Srinivasan et al. 2009). Observational

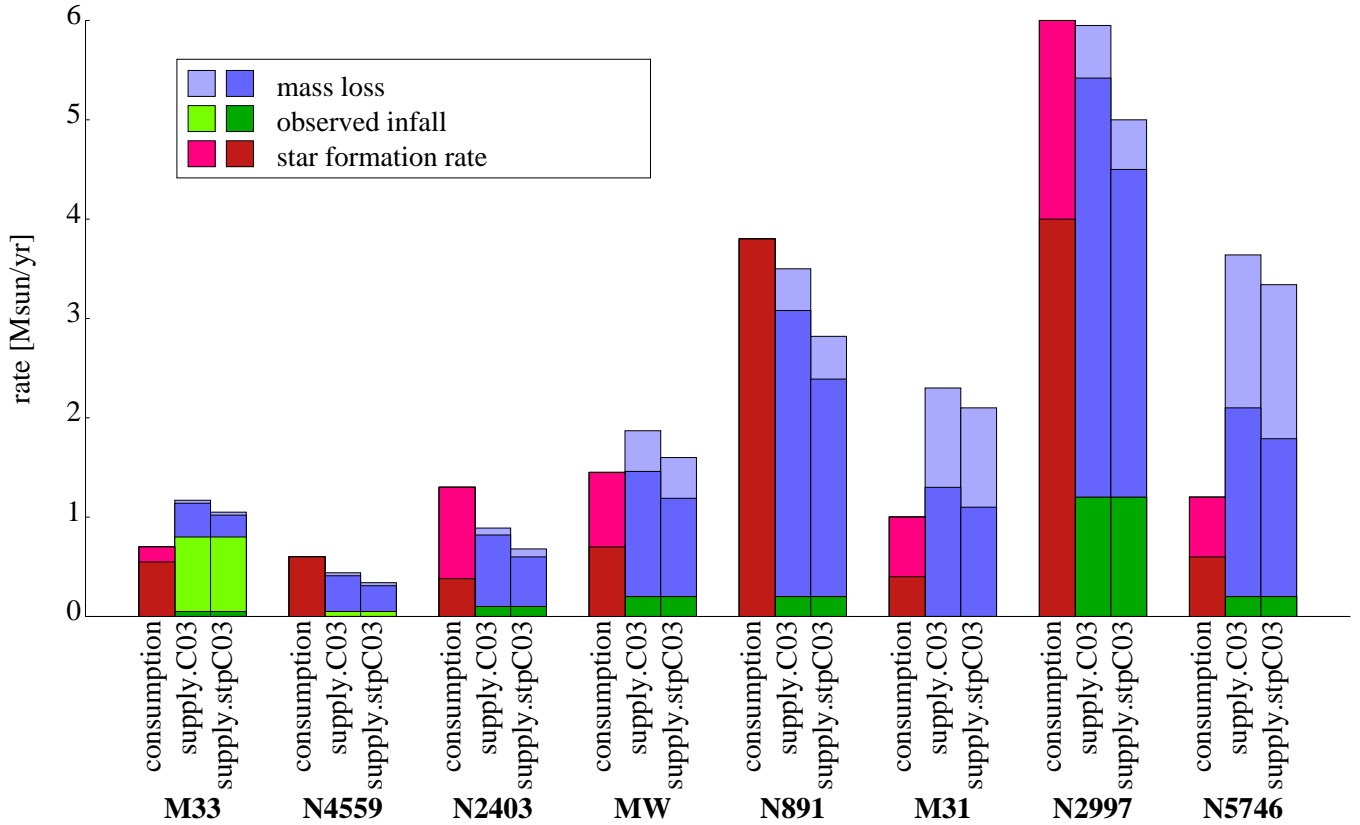


Figure 7. The gas budget for each galaxy labeled on the bottom axis. Bars on the left of each galaxy denote the observed gas consumption from star formation (dark red and magenta). The two sets of bars on the right denote gas supplied from observed infall of new gas (green) and stellar mass loss (blue). The two gas supply rate columns are labeled, below, by the C03 and stpC03 IMFs on which they are based. The lighter shades of each quantity indicate the space between low and high estimates of that quantity. For stellar mass loss, these are based on the uncertainty estimates from this study; for star formation and infall, they are based on the size of cited error bars and scatter between different measurements. Specific values, references and notes are given in Table 2.

Table 2
Galaxy properties and the gas budget.

Galaxy	M_{*0}^a ($10^9 M_{\odot}$)	v_{flat} (km s^{-1})	median(SFR ₀) ($M_{\odot} \text{ yr}^{-1}$)	SFR ₀ ^a ($M_{\odot} \text{ yr}^{-1}$)	Accretion rate ^b ($M_{\odot} \text{ yr}^{-1}$)	Stellar Mass Loss Rates C03 ($M_{\odot} \text{ yr}^{-1}$)	stpc03 ($M_{\odot} \text{ yr}^{-1}$)	References [M_{*0}][SFR ₀][Accr.]
M33	4.5	104	0.42	0.55 – 0.7	0.05 – 0.8 ^c	0.34-0.37	0.22-0.25	[1][2,3][4]
NGC 4559	6.8	123	0.58	0.6	< 0.05	0.36-0.39	0.26-0.29	[5][6][7]
NGC 2403	5-14	134	1.0	0.38-1.3	0.1	0.72-0.79	0.50-0.58	[8,9][10,11][12]
Milky Way	55	220	2.8	0.7 – 1.45	0.2	1.26-1.67	0.99-1.40	[13][14,15][16]
NGC 891 .	100	230	4.3	3.8	0.2 ^d	2.88-3.30	2.19-2.62	[17][18][19]
M31	100	260	4.3	0.4 – 1.0	0.0	1.30-2.30	1.10-2.10	[20][21,22,23][24]
NGC 2997	160	226	6.2	5.0 ± 1	1.2	4.22-4.75	3.30-3.80	[25][26][27]
NGC 5746	160	320	6.2	0.8 ± 0.2 – 1.2	0.2	1.90-3.44	1.59-3.14	[28][29,30][31]

^aSystematic and random errors in stellar mass and SFR are likely $\lesssim 0.3\text{dex}$ (Mo et al. 2010), but difference between stellar masses and SFR derived with C03 and stpC03 should be $< 10\%$ (approximately the difference between the Kroupa et al. 1993 and Kroupa 2001 IMFs found by Borch et al. 2006). ^bAccretion rates are probably lower limits to cold-gas accretion, and do not include helium or ionized gas fractions unless noted. ^cInfall of surrounding gas clouds at 100 km s^{-1} is assumed, the low (high) value excludes (includes) an ionization correction; ^dIf all HI in the halo of NGC 891 were to fall toward the disk it would supply $\sim 30 M_{\odot} \text{ yr}^{-1}$;

References: [1] Corbelli (2003); [2] Magrini et al. (2007); [3] Blitz & Rosolowsky (2006); [4] Grossi et al. (2008); [5] Barbieri et al. (2005), from M_{*}/L_k ; [6] Fraternali (2010); [7] Barbieri et al. (2005); [8] Leroy et al. (2008); [9] de Blok & McGaugh (1996); [10] Leroy et al. (2008); [11] Kennicutt et al. (2003); [12] Fraternali et al. (2002); [13] Flynn et al. (2006); [14] Robitaille & Whitney (2010); [15] Murray & Rahman (2010); [16] Wakker et al. (2007); [17] Rhode et al. (2010); [18] Popescu et al. (2004); [19] Oosterloo et al. (2007); [20] Chemin et al. (2009); [21] Walterbos & Braun (1994); [22] Barmby et al. (2006); [23] Williams (2003); [24] Chemin et al. (2009); [25] Louise & Marcelin (1983); [26] Hess et al. (2009); [27] Hess et al. (2009); [28] Rasmussen et al. (2009); [29] Rasmussen et al. (2006); [30] Pedersen et al. (2006); [31] Rand & Benjamin (2008);

estimates of total mass loss from the AGB stars for these galaxies range from $\sim 10\%$ (LMC) to $\sim 50 - 100\%$ (WLM,

IC 1613) of their total SFR. Given that additional mass loss can be expected from supernovae and red giant stars, these in-

dependent, direct estimates are consistent with our model calculations and also suggest that stellar mass loss may provide substantial fuel for ongoing star formation in these galaxies.

5. DISCUSSION AND CONCLUSIONS

We have used a simple, empirically-motivated model for deriving star formation histories of galaxies of different stellar masses along with mass loss rates from stellar evolution code to show that stellar mass loss can be the most important source of gas for fueling continuing star formation in late type galaxies at low redshifts ($z \lesssim 0.1 - 0.5$). We also explicitly show that the gas supplied by stellar mass loss is comparable to the perceived deficit of gas required to fuel continuing star formation in a number of nearby galaxies. This conclusion is consistent with direct observational estimates of stellar mass loss contribution of gas to the ISM of nearby dwarf galaxies, such as WLM and IC1613. We presented tests of the effects of scatter and uncertainties in the SFR- M_* relation on our results and have show that our conclusions are not affected.

We believe that our calculations provide a conservative estimate of the expected stellar mass loss rates. First, they rely on star formation histories derived from the *observed* evolution of the SFR- M_* relation. Thus, only if current observational results on the evolution of this relation are significantly biased, would our conclusions be biased as well. Moreover, in the Appendix we show that any feedback that delays consumption of material lost by stars will only further enhance the rate that recycled gas gets reprocessed at late epochs.

Maintaining a gas supply for star formation at $z \approx 0$ primarily through recycled stellar mass has implications for the recent chemical enrichment histories of galaxies. In the case of the Milky Way, ongoing infall of pristine gas is thought to be required to match the observed enrichment history and metallicity distribution (e.g., Sancisi et al. 2008). However, observations of the Milky Way and other nearby galaxies show that the metallicities of planetary nebulae are generally lower than or equal to the metallicities of the HII regions around young stars (Stanghellini et al. 2010), meaning that gas returned to the ISM by such nebulae does not need to be diluted by infall in order to provide fuel for currently forming stars. Furthermore, detailed enrichment models are actually not so restrictive at late epochs. For example, Chiappini (2008) points out that although chemical evolution models show a need for large inflow rates during the early stages of the evolution of the Milky Way disk, a present day infall rate of only $\approx 0.45 M_\odot \text{ yr}^{-1}$ is used in the fiducial Chiappini et al. (2001) model that is consistent with enrichment constraints.

Deuterium abundances can potentially provide the most stringent constraint on the amount of gas that stellar mass loss can supply to galaxies like the Milky Way. Deuterium is completely destroyed in stars, so that the deuterium abundance in the ISM of a galaxy relative to its primordial value constrains the fraction of ISM recycled through stars (see, e.g., Pagel 2009, for a pedagogical review and Prodanović et al. 2010 for a recent analysis). However, it is not clear how restrictive deuterium constraints are at present. Deuterium abundance exhibits variation of a factor of $\sim 3 - 4$ even within a kiloparsec from the Sun (Sonneborn et al. 2000; Linsky et al. 2006) and longer lines of sight indicate lower abundances (Wood et al. 2004). One possible interpretation is that variation of deuterium abundance is due to its depletion onto dust grains (Linsky et al. 2006), in which case the largest observed abundances should be interpreted as the true undepleted val-

ues. Such assumption leads to conclusion that most of the present ISM gas in the Milky Way should be unprocessed by stars (Prodanović & Fields 2008; Prodanović et al. 2010). However, while dust depletion interpretation of observed deuterium abundance variation is plausible, some puzzles do remain. For example, the correlation between deuterium abundance along a line of sight and reddening in the same direction, which would be expected within such framework, has not been detected (Steigman et al. 2007). This implies that abundance variation may also be due to incomplete ISM mixing, in which case the constraints on recycled fraction can be substantially relaxed. Finally, we note also that in the context of this study, the deuterium abundance in the solar neighborhood may not be representative for the global constraints for the entire Galaxy. This is because most of molecular gas and star formation in the Milky Way occurs in a ring at $\sim 3 - 6$ kpc from the Galactic center and the deuterium abundance in that region is substantially lower than around the Sun (Lubowich & Pasachoff 2010).

An interesting implication of our results is that stars can be forming largely from recycled stellar material for cosmologically significant periods of time. The question is then why some galaxies with significant stellar mass do not form stars during late stages of their evolution. Although some cold gas is observed in early type galaxies (e.g., Bouchard et al. 2005; Welch et al. 2010), most elliptical galaxies have star formation rates much lower than the expected rate of stellar mass loss. Although detailed analysis of this issue is beyond the scope of this study, the likely explanation is that gas lost by stars in spheroidal systems orbiting with high velocities within tenuous hot halo is efficiently mixed with halo gas. The situation is analogous to a well-known “cloud in the wind” problem (e.g., Agertz et al. 2007) with hot halo gas acting as high-velocity wind blowing past a red giant envelope. The cloud is expected to be unstable to the Kelvin-Helmholz (KH) instability and to be disrupted and mixed with hot gas on a short time scale. The extent of this mixing is a subject of active research (Bregman & Parriott 2009; Parriott & Bregman 2008). At the center of early types, densities of recycled material should become so high that only regular AGN activity may keep recycled material from condensing (Ciotti & Ostriker 2007). Interestingly, the abundance of dust expected to come from the envelopes of red giant stars according to stellar mass loss models is also not observed in nearby globular clusters (e.g., Barmby et al. 2009; Gnedin et al. 2002; van Loon et al. 2009). In this case, globular cluster stars are also moving through Milky Way halo gas at high velocity, so no accumulation of cold gas shed by stars may be possible as that gas is, again, experiencing ram pressure, KH instabilities, and mixing (e.g., van Loon et al. 2009).

The situation is likely to be different for disk galaxies because disk stars are releasing their gas directly into co-rotating ISM, rather than rapidly flowing hot halo gas. The lost gas can therefore join ISM and become readily available for star formation. Therefore, our results and conclusions about importance of stellar mass loss should be primarily applicable to late-type disk galaxies. In this respect, it is interesting that observations indicate that there is more gas in the luminous S0 galaxies than in the elliptical galaxies of similar luminosity (Welch et al. 2010).

Even in the disk systems, however, the stellar mass loss may only be efficient in fueling star formation in the presence of at least some gaseous disk. Gas lost by stars in a pure stellar disk (without any corotating gas) would be subject to the

same efficient mixing with halo gas, as stars that are moving with high velocities through slowly rotating halo. Therefore, stellar mass loss may become inefficient in fueling continuing star formation when gas surface densities falls to some small value.

The significant role of stellar mass loss in fueling continuing star formation during late stages of evolution of galaxies implies that it is very important to include this process in cosmological simulations of galaxy formation. Inclusion of stellar mass loss in simulations is straightforward: for a given choice of IMF, the mass of gas returned to ISM in a given interval of time is given by the differential of equation 1 with appropriate parameters (see Table 1). This mass can be added directly to a host cell of stellar particle in a grid simulation or distributed over neighboring gas particles in SPH simulations. Simulations with and without stellar mass loss can be used to explore other possible effects of this process, such as effect on galaxy morphologies (Martig & Bournaud 2010) and their stellar masses. The latter will depend on the star formation histories of galaxies and thus may exhibit systematic variation with host halo mass and contribute to the scatter of stellar mass at a fixed halo mass.

APPENDIX

MODELING GAS REPROCESSING

Until now we have dealt with mass loss from a stellar population at a particular instant, ignoring that gas returned to ISM may not be immediately accessible to form stars and may instead accumulate. Using cosmological galaxy formation simulations, we now address issue of how much gas might be available from stellar recycling to be reprocessed to form stars at low redshift, given gas reprocessing physics over galaxy’s mass loss history.

Simulations

Cosmological galaxy formation simulations of MW-sized systems were carried out using Eulerian, gas dynamics+ N -body adaptive refinement tree (ART) code (Kravtsov 1999; Kravtsov et al. 2002; Rudd et al. 2008). The simulations followed the evolution of dark matter and baryons in a box of comoving size $L_{\text{box}} = 20h^{-1}$ Mpc in a flat Λ CDM cosmology: $\Omega_0 = 1 - \Omega_\Lambda = 0.258$, $\Omega_b = 0.044$, $h = 0.72$, $n_s = 0.96$, $\sigma_8 = 0.80$

A standard “zoom-in” approach was used to generate initial conditions in order to achieve high mass resolution, while adaptive mesh refinement was used to increase the spatial resolution in regions where baryons collapse to form galactic disks. Milky Way-sized systems were selected for resimulation from a low-resolution non-radiative simulation at $z = 0$. Particles within three virial radii of the center of each object were then replaced at the initial epoch ($z = 62$) with eight times more high-resolution particles of mass $m_{\text{DM}} = 2.82 \times 10^7 h^{-1} M_\odot$ with a spatial distribution constrained to match the low resolution initial conditions, while also including additional smaller scale power. There is no contamination by low resolution dark matter particles within the virial radius of our halos at $z = 0$, but the large-scale tidal field remains accurately sampled using this technique.

The simulation box was initially resolved by a uniform 128^3 grid and additional successive refinements were introduced in collapsing regions that were occupied by the high-resolution dark matter particles. The cells were refined if their gas mass exceeded $m_b = 4.67 \times 10^7 h^{-1} M_\odot$ or the dark matter mass in a cell is more than $2m_{\text{DM}}$, where m_{DM} is the mass of the highest resolution dark matter particle. Cells are $610h^{-1}$ pc across in comoving units at the maximum allowed refinement level.

Five Milky Way size halos were simulated to $z = 0$. In order to isolate the effects of mass loss, simulations of each halo were run with mass loss turned on (ml) and mass loss turned off (nml). We required that the sample halos did not undergo major mergers after a lookback time of 5 Gyr and that simulations of the same halo with ml and nml did not differ significantly in accretion or timing of mergers (e.g., Frenk et al. 1999) as a result of the differing physics. Two halos met these criteria and they are presented here as MW1 and MW2. They have final total masses of $M_{\text{MW1}} = 1.6 \times 10^{12} h^{-1} M_\odot$ and $M_{\text{MW2}} = 1.9 \times 10^{12} h^{-1} M_\odot$ at overdensity $\rho = 200\rho_{\text{cr}}$, where ρ_{cr} is the critical density of the universe at the epoch of analysis.

Subgrid Physics

Star formation is modeled in our simulations with a simple density dependence and efficiency:

$$\dot{\rho}_* = \frac{\rho_{\text{gas}}}{\tau_*} \left(\frac{\rho_{\text{gas}}}{0.01 M_\odot \text{pc}^{-3}} \right)^{0.5}$$

, and we adopt $\tau_* = 4$ Gyr, noting that the results and our conclusions are not very sensitive to the exact value of τ_* . Stellar particles are allowed to form in regions with density above threshold value of $n_{\text{sf}} = 0.5 \text{ cm}^{-3}$ and a temperature below the threshold value of $T_{\text{sf}} < 9000$ K. Such a high temperature and low density thresholds are reasonable choices for simulations of relatively low spatial resolution that we use in this study (see Saitoh et al. 2008, for a discussion of τ_* , n_{sf} , and T_{sf}).

ACKNOWLEDGMENTS

We are grateful to Mary Putman, Oleg Gnedin, Marcel Haas, Don York and Donald Lubowich for useful discussions and comments, to Nick Gnedin for providing the code to generate initial conditions for the cosmological simulations used in the appendix, and to the the anonymous referee for helpful suggestions. This work was partially supported by and by the NSF grant AST-0708154 and by the Kavli Institute for Cosmological Physics at the University of Chicago through the NSF grant PHY-0551142 and an endowment from the Kavli Foundation. The simulations used in this work have been performed on the Joint Fermilab - KICP Supercomputing Cluster, supported by grants from Fermilab, Kavli Institute for Cosmological Physics, and the University of Chicago. This work made extensive use of the NASA Astrophysics Data System and arXiv.org preprint server. AK would like to thank the Aspen Center for Physics and organizers of the “Star formation in galaxies” workshop for hospitality and stimulating and productive atmosphere during the completion of this paper.

Each newly formed stellar particle is treated as an SSP with a stellar initial mass function (IMF) that is described by the Miller & Scalo (1979) functional form, with stellar masses in the range $0.1 - 100M_{\odot}$. All stars with $M_* > 8M_{\odot}$ immediately deposit both 2×10^{51} ergs of thermal energy, accounting for the energy input by stellar winds and type II supernova (SN II), and a fraction $f_Z = \min(0.2, \frac{0.01M_*}{M_{\odot}} - 0.06)$ of their mass as metals, into the surrounding gas, in order to approximate the results of Woosley & Weaver (1995). The code also accounts for the SN Ia feedback, assuming a rate that slowly increases with time and broadly peaks at the population age of 1 Gyr. We assume that a fraction of 1.5×10^{-2} of mass in stars between 3 and $8M_{\odot}$ explodes as SN Ia over the entire population history and that each SN Ia dumps 2×10^{51} erg of thermal energy and ejects $1.3M_{\odot}$ of metals into the surrounding gas. For the assumed IMF, 75 SN II (instantly) and 11 SN Ia (over several billion years) are produced by a 10^4M_{\odot} stellar particle. This sort of model, without ad hoc kicks or delayed cooling, has been shown to have a negligible effect on the SFH and resulting galaxy properties compared to a model without feedback (Katz 1992; Tassis et al. 2008; Schaye et al. 2010). Metallicity dependent equilibrium cooling rates, as well as UV heating rates, due to the cosmological ionizing background, are tabulated using the Cloudy code (Ferland et al. 1998, v96b4).

The stellar mass loss of each stellar particle is modeled using eq. 1 with $C_0 = 0.05$ and $\lambda = 5$ Myr and about 40% of initial mass of stellar particle is lost over a Hubble time with these parameters. At each time step, gas mass lost by a stellar particle is added to gas of its parent cell along with its energy and momentum. The interpretation of our simulation results is not sensitive to the specific choice of C_0 and λ .

As a result of the known problems with simple galaxy formation simulations, our galaxies overcool and produce stellar fractions that are about 5 times too high compared to observational expectations. To account for this, we re-normalize all star formation histories of the simulated galaxies with the constant ratio of the final stellar mass in the *ml* simulation to the Milky Way value of $5.5 \times 10^{10}M_{\odot}$ (e.g., Flynn et al. 2006).

Gas Reprocessing Results

The star formation histories of our two simulated galaxies are plotted in Figure 8. There are no major mergers after $z = 0.5$, and these SFHs show few sustained bursts, making their growth largely consistent with expectations for the build up of the Milky Way (e.g., Rocha-Pinto et al. 2000). The SFHs show that $z = 0$ SFRs in the runs with mass loss (*ml* plotted in red) are more than a factor of two higher than the SFRs in the corresponding simulations without mass loss (*nml* plotted in blue). This confirms the basic expectation that gas lost by stars can be a significant source of fuel for star formation at low redshift.

We use the *nml* simulation to test whether simple assumptions about the fate of gas lost by stars can reproduce results of simulations with stellar mass loss. The GMLR is given by eq. 3, however, the gas returned to the ISM can accumulate and be consumed over a certain gas consumption time scale. The mass that accumulates in the ISM from stellar mass loss between time t_0 and t is then

$$m_{\text{ml}}(t_0, t) = \int_{t_0}^t \{\text{GMLR}(t') - [\text{SFR}(t') - \text{SFR}_{\text{nml}}(t')]\} dt' \quad (\text{A1})$$

To determine the SFR and hence a stellar mass loss rate, we assume a linear SFR scaling with gas density that has a gas consumption time scale τ_{gc} . Enhancement in star formation is therefore directly proportional to mass added to the star forming ISM,

$$\text{SFR}(t) = \text{SFR}_{\text{nml}}(t) + \frac{m_{\text{ml}}(0, t)}{\tau_{\text{gc}}} \quad (\text{A2})$$

Stars formed from the gas lost by stars will themselves lose mass, and this mass will, in turn form stars. In order to fully account for the additional star formation resulting from mass loss, equation A2 needs to be iterated when starting from the *nml* case, replacing $\text{SFR}_{\text{nml}}(t)$ with each subsequent $\text{SFR}(t)$, until $\text{SFR}(t)$ converges.

The simulation's true star formation law is nonlinear in density, meaning that τ_{gc} effectively varies with density. The average gas densities of a star forming disk in simulations can vary from $\tau_{\text{gc}} = 500$ Myr to a τ_{gc} of few billion years, with stars tending to form in lower density gas (longer τ_{gc}) as accretion slows and the gas in their disks is depleted. However, this change in the efficiency of gas conversion occurs slowly and, furthermore, the effect of τ_{gc} is mitigated by the fact that a reduction in τ_{gc} results in a build up of $m_{\text{ml}}(0, t)$, which leads to more star formation. A constant τ_{gc} therefore mimics the relevant behavior.

An alternative, simpler model, which we will call *instant reprocessing*³, can be constructed by taking τ_{gc} to 0. Then gas returned to ISM by stars is immediately consumed by star formation so only ongoing mass loss contributes to star formation and thus

$$\text{SFR}(t) = \text{SFR}_{\text{nml}}(t) + \text{GMLR}(t). \quad (\text{A3})$$

We plot SFHs with both a $\tau_{\text{gc}} = 1$ Gyr, and instantaneous reprocessing applied to the SFH from the *nml* simulation in Figure 8. The mapping between simulations is not exact. Gas returned during a merger may be returned to the diffuse halo and be temporarily lost to the star forming disk. Nonetheless, throughout most of its lifetime, and especially in late epochs when the galaxy is quiescently evolving, the simple assumption of instant reprocessing applied to the *nml* simulations generates an excellent match to the SFH in the *ml* simulations.

Reprocessing models with longer gas consumption timescales result in gas accumulation and more gas reprocessing at late times, because they smooth the declining reprocessing rate curve. For the simulated SFHs, the effect of the $\tau_{\text{gc}} = 1$ Gyr reprocessing is a $\lesssim 10\%$ enhancement in SFRs at late epochs compared to the instantaneous reprocessing model. It is worth

³ Instant reprocessing is distinct from the instant recycling approximation. Instant *recycling* approximates mass loss as instantaneous (e.g., Tinsley 1980), whereas instant *reprocessing* approximates the birth of stars from returned material as instantaneous.

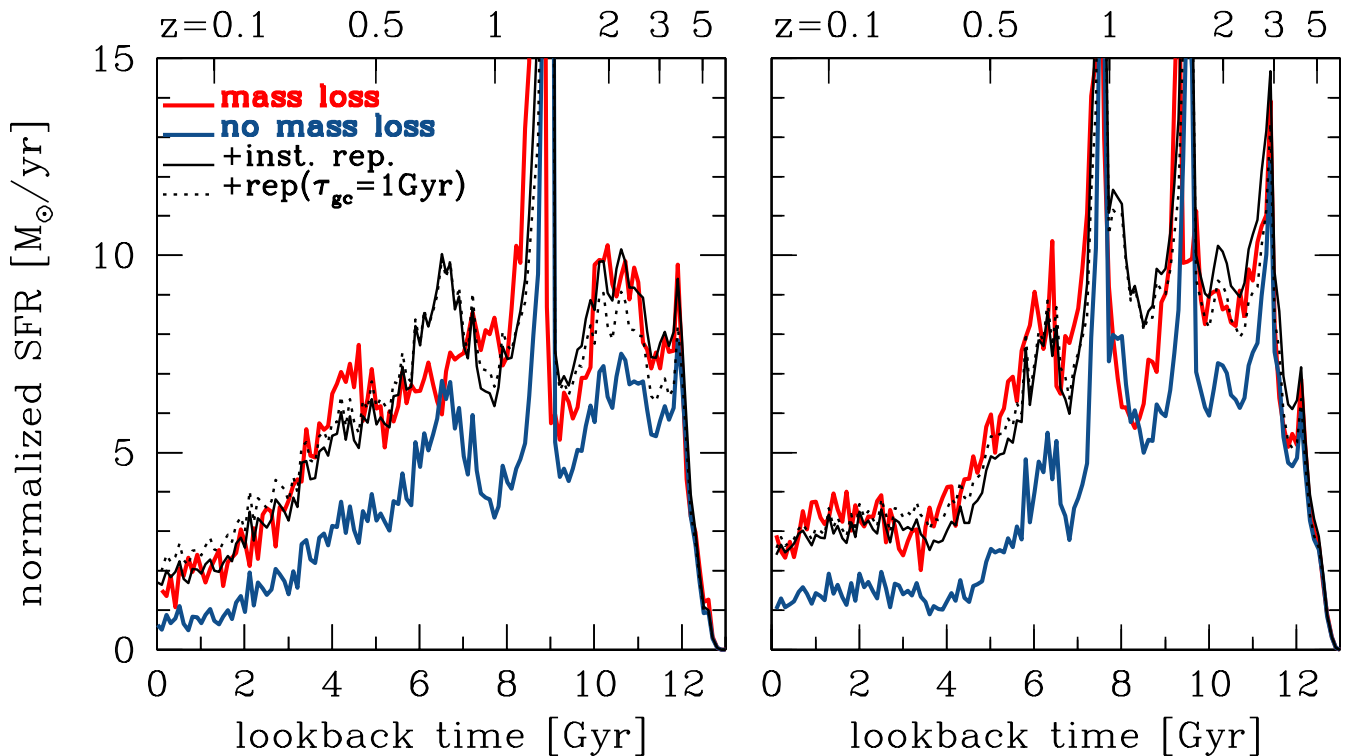


Figure 8. Simulated SFHs that include all stars within $30h^{-1}$ kpc of the galaxy and are normalized in such a way that the final stellar mass is equal to $5.5 \times 10^{10} M_{\odot}$. The thin blue lines are SFHs for simulations that do not include mass loss from stars (*nml*), while the thick red line is a fiducial simulation with mass loss included (*ml*). Black lines are gas recycling models, with gas consumption timescales $\tau_{gc} = 0$ Gyr (solid) and $\tau_{gc} = 1$ Gyr (dotted), that attempt to map the *nml* SFH onto the *ml* SFH.

emphasizing that any feedback mechanism that slows the processing of gas to stars would have the effect of raising τ_{gc} and would therefore imply a higher rate of gas reprocessing at late epochs.

REFERENCES

- Agertz, O., Moore, B., Stadel, J., Potter, D., Miniati, F., Read, J., Mayer, L., Gawryszczak, A., Kravtsov, A., Nordlund, Å., Pearce, F., Quilis, V., Rudd, D., Springel, V., Stone, J., Tasker, E., Teyssier, R., Wadsley, J., & Walder, R. 2007, *MNRAS*, 380, 963
- Agertz, O., Teyssier, R., & Moore, B. 2010, arXiv:1004.0005
- Barbieri, C. V., Fraternali, F., Oosterloo, T., Bertin, G., Boomsma, R., & Sancisi, R. 2005, *A&A*, 439, 947
- Barmby, P., Ashby, M. L. N., Bianchi, L., Engelbracht, C. W., Gehrz, R. D., Gordon, K. D., Hinz, J. L., Huchra, J. P., Humphreys, R. M., Pahre, M. A., Pérez-González, P. G., Polomski, E. F., Rieke, G. H., Thilker, D. A., Willner, S. P., & Woodward, C. E. 2006, *ApJ*, 650, L45
- Barmby, P., Boyer, M. L., Woodward, C. E., Gehrz, R. D., van Loon, J. T., Fazio, G. G., Marengo, M., & Polomski, E. 2009, *AJ*, 137, 207
- Bastian, N., Covey, K. R., & Meyer, M. R. 2010, arXiv:1001.2965
- Bauermeister, A., Blitz, L., & Ma, C. 2010, *ApJ*, 717, 323
- Bell, E. F. & de Jong, R. S. 2001, *ApJ*, 550, 212
- Bell, E. F., Zheng, X. Z., Papovich, C., Borch, A., Wolf, C., & Meisenheimer, K. 2007, *ApJ*, 663, 834
- Bigiel, F., Leroy, A., Walter, F., Brinks, E., de Blok, W. J. G., Madore, B., & Thornley, M. D. 2008, *AJ*, 136, 2846
- Bland-Hawthorn, J. 2009, in *IAU Symposium*, Vol. 254, *IAU Symposium*, ed. J. Andersen, J. Bland-Hawthorn, & B. Nordström, 241–254
- Blitz, L. 1997, in *IAU Symposium*, Vol. 170, *IAU Symposium*, ed. W. B. Latter, S. J. E. Radford, P. R. Jewell, J. G. Mangum, & J. Bally, 11–18
- Blitz, L. & Rosolowsky, E. 2006, *ApJ*, 650, 933
- Blitz, L., Spergel, D. N., Teuben, P. J., Hartmann, D., & Burton, W. B. 1999, *ApJ*, 514, 818
- Borch, A., Meisenheimer, K., Bell, E. F., Rix, H., Wolf, C., Dye, S., Kleinheinrich, M., Kovacs, Z., & Wisotzki, L. 2006, *A&A*, 453, 869
- Bouchard, A., Jerjen, H., Da Costa, G. S., & Ott, J. 2005, *AJ*, 130, 2058
- Bouché, N., Dekel, A., Genzel, R., Genel, S., Cresci, G., Förster Schreiber, N. M., Shapiro, K. L., Davies, R. I., & Tacconi, L. 2010, *ApJ*, 718, 1001
- Bregman, J. N. & Parriott, J. R. 2009, arXiv:0907.3489
- Brinchmann, J., Charlot, S., White, S. D. M., Tremonti, C., Kauffmann, G., Heckman, T., & Brinkmann, J. 2004, *MNRAS*, 351, 1151
- Cappellari, M., Bacon, R., Bureau, M., Damen, M. C., Davies, R. L., de Zeeuw, P. T., Emsellem, E., Falcón-Barroso, J., Krajnović, D., Kuntschner, H., McDermid, R. M., Peletier, R. F., Sarzi, M., van den Bosch, R. C. E., & van de Ven, G. 2006, *MNRAS*, 366, 1126
- Chabrier, G. 2001, *ApJ*, 554, 1274
- , 2003, *PASP*, 115, 763
- Chemin, L., Carignan, C., & Foster, T. 2009, *ApJ*, 705, 1395
- Chiappini, C. 2008, in *Astronomical Society of the Pacific Conference Series*, Vol. 396, *Astronomical Society of the Pacific Conference Series*, ed. J. G. Funes & E. M. Corsini, 113–+
- Chiappini, C., Matteucci, F., & Romano, D. 2001, in *Astronomical Society of the Pacific Conference Series*, Vol. 230, *Galaxy Disks and Disk Galaxies*, ed. J. G. Funes & E. M. Corsini, 83–84
- Ciotti, L. & Ostriker, J. P. 2007, *ApJ*, 665, 1038
- Conroy, C. & Gunn, J. E. 2010, *ApJ*, 712, 833
- Conroy, C. & Wechsler, R. H. 2009, *ApJ*, 696, 620

- Corbelli, E. 2003, *MNRAS*, 342, 199
- Daddi, E., Bournaud, F., Walter, F., Dannerbauer, H., Carilli, C. L., Dickinson, M., Elbaz, D., Morrison, G. E., Riechers, D., Onodera, M., Salmi, F., Krips, M., & Stern, D. 2010a, *ApJ*, 713, 686
- Daddi, E., Dannerbauer, H., Stern, D., Dickinson, M., Morrison, G., Elbaz, D., Giavalisco, M., Mancini, C., Pope, A., & Spinrad, H. 2009, *ApJ*, 694, 1517
- Daddi, E., Dickinson, M., Morrison, G., Chary, R., Cimatti, A., Elbaz, D., Frayer, D., Renzini, A., Pope, A., Alexander, D. M., Bauer, F. E., Giavalisco, M., Huynh, M., Kurk, J., & Mignoli, M. 2007, *ApJ*, 670, 156
- Daddi, E., Elbaz, D., Walter, F., Bournaud, F., Salmi, F., Carilli, C., Dannerbauer, H., Dickinson, M., Monaco, P., & Riechers, D. 2010b, *ApJ*, 714, L118
- Davé, R. 2008, *MNRAS*, 385, 147
- Davé, R., Finlator, K., Oppenheimer, B. D., Fardal, M., Katz, N., Kereš, D., & Weinberg, D. H. 2010, *MNRAS*, 404, 1355
- de Blok, W. J. G. & McGaugh, S. S. 1996, *ApJ*, 469, L89+
- Dekel, A., Birnboim, Y., Engel, G., Freundlich, J., Goerdt, T., Mumcuoglu, M., Neistein, E., Pichon, C., Teyssier, R., & Zinger, E. 2009, *Nature*, 457, 451
- Drory, N. & Alvarez, M. 2008, *ApJ*, 680, 41
- Dutton, A. A., van den Bosch, F. C., & Dekel, A. 2010, *MNRAS*, 608
- Elbaz, D., Daddi, E., Le Borgne, D., Dickinson, M., Alexander, D. M., Chary, R., Starck, J., Brandt, W. N., Kitzbichler, M., MacDonald, E., Nonino, M., Popesso, P., Stern, D., & Vanzella, E. 2007, *A&A*, 468, 33
- Erb, D. K., Steidel, C. C., Shapley, A. E., Pettini, M., Reddy, N. A., & Adelberger, K. L. 2006, *ApJ*, 647, 128
- Faucher-Giguere, C., Keres, D., & Ma, C. 2011, *ArXiv e-prints*
- Ferland, G. J., Korista, K. T., Verner, D. A., Ferguson, J. W., Kingdon, J. B., & Verner, E. M. 1998, *PASP*, 110, 761
- Flynn, C., Holmberg, J., Portinari, L., Fuchs, B., & Jahreiß, H. 2006, *MNRAS*, 372, 1149
- Fraternali, F. 2009, in *IAU Symposium*, Vol. 254, *IAU Symposium*, ed. J. Andersen, J. Bland-Hawthorn, & B. Nordström, 255–262
- Fraternali, F. 2010, in *American Institute of Physics Conference Series*, Vol. 1240, *American Institute of Physics Conference Series*, ed. V. P. Debattista & C. C. Popescu, 135–145
- Fraternali, F. & Binney, J. J. 2008, *MNRAS*, 386, 935
- Fraternali, F., van Moorsel, G., Sancisi, R., & Oosterloo, T. 2002, *AJ*, 123, 3124
- Frenk, C. S., White, S. D. M., Bode, P., Bond, J. R., Bryan, G. L., Cen, R., Couchman, H. M. P., Evrard, A. E., Gnedin, N., Jenkins, A., Khokhlov, A. M., Klypin, A., Navarro, J. F., Norman, M. L., Ostriker, J. P., Owen, J. M., Pearce, F. R., Pen, U., Steinmetz, M., Thomas, P. A., Villumsen, J. V., Wadsley, J. W., Warren, M. S., Xu, G., & Yepes, G. 1999, *ApJ*, 525, 554
- Genzel, R., Tacconi, L. J., Gracia-Carpio, J., & et al. 2010, *MNRAS in press* (arXiv/1003.5180)
- Girardi, L., Bressan, A., Bertelli, G., & Chiosi, C. 2000, *A&AS*, 141, 371
- Gnedin, O. Y., Zhao, H., Pringle, J. E., Fall, S. M., Livio, M., & Meylan, G. 2002, *ApJ*, 568, L23
- González, V., Labbé, I., Bouwens, R. J., Illingworth, G., Franx, M., Kriek, M., & Brammer, G. B. 2010, *ApJ*, 713, 115
- Greivich, J. & Putman, M. E. 2009, *ApJ*, 696, 385
- Groenewegen, M. A. T., Wood, P. R., Sloan, G. C., Blommaert, J. A. D. L., Cioni, M., Feast, M. W., Hony, S., Matsuura, M., Menzies, J. W., Olivier, E. A., Vanhollebeke, E., van Loon, J. T., Whitelock, P. A., Zijlstra, A. A., Habing, H. J., & Lagadec, E. 2007, *MNRAS*, 376, 313
- Grossi, M., Giovanardi, C., Corbelli, E., Giovanelli, R., Haynes, M. P., Martin, A. M., Saintonge, A., & Dowell, J. D. 2008, *A&A*, 487, 161
- Heitsch, F. & Putman, M. E. 2009, *ApJ*, 698, 1485
- Hess, K. M., Pisano, D. J., Wilcots, E. M., & Chengalur, J. N. 2009, *ApJ*, 699, 76
- Hill, A. S., Haffner, L. M., & Reynolds, R. J. 2009, *ApJ*, 703, 1832
- Hurley, J. R., Pols, O. R., & Tout, C. A. 2000, *MNRAS*, 315, 543
- Jackson, D. C., Skillman, E. D., Gehrz, R. D., Polomski, E., & Woodward, C. E. 2007a, *ApJ*, 656, 818
- . 2007b, *ApJ*, 667, 891
- Jungwiert, B., Combes, F., & Palouš, J. 2001, *A&A*, 376, 85
- Kalirai, J. S., Hansen, B. M. S., Kelson, D. D., Reitzel, D. B., Rich, R. M., & Richer, H. B. 2008, *ApJ*, 676, 594
- Katz, N. 1992, *ApJ*, 391, 502
- Katz, N., Weinberg, D. H., & Hernquist, L. 1996, *ApJS*, 105, 19
- Kauffmann, G., Li, C., & Heckman, T. M. 2010, *arXiv:1005.1825*
- Kennicutt, Jr., R. C. 1998, *ApJ*, 498, 541
- Kennicutt, Jr., R. C., Armus, L., Bendo, G., Calzetti, D., Dale, D. A., Draine, B. T., Engelbracht, C. W., Gordon, K. D., Grauer, A. D., Helou, G., Hollenbach, D. J., Jarrett, T. H., Kewley, L. J., Leitherer, C., Li, A., Malhotra, S., Regan, M. W., Rieke, G. H., Riecke, M. J., Roussel, H., Smith, J., Thornley, M. D., & Walter, F. 2003, *PASP*, 115, 928
- Kennicutt, Jr., R. C., Tamblyn, P., & Congdon, C. E. 1994, *ApJ*, 435, 22
- Kereš, D. & Hernquist, L. 2009, *ApJ*, 700, L1
- Knapp, G. R. 1990, in *Astrophysics and Space Science Library*, Vol. 161, *The Interstellar Medium in Galaxies*, ed. H. A. Thronson Jr. & J. M. Shull, 3–37
- Kravtsov, A. V. 1999, PhD thesis, New Mexico State University
- Kravtsov, A. V. & Gnedin, O. Y. 2005, *ApJ*, 623, 650
- Kravtsov, A. V., Klypin, A., & Hoffman, Y. 2002, *ApJ*, 571, 563
- Kroupa, P. 2001, *MNRAS*, 322, 231
- . 2007, *ArXiv Astrophysics e-prints*
- Kroupa, P., Gilmore, G., & Tout, C. A. 1991, *MNRAS*, 251, 293
- Kroupa, P., Tout, C. A., & Gilmore, G. 1993, *MNRAS*, 262, 545
- Kroupa, P. & Weidner, C. 2003, *ApJ*, 598, 1076
- Leitner, S. N. 2011
- Leroy, A. K., Walter, F., Brinks, E., Bigiel, F., de Blok, W. J. G., Madore, B., & Thornley, M. D. 2008, *AJ*, 136, 2782
- Libert, Y., Gérard, E., Thum, C., Winters, J. M., Matthews, L. D., & Le Bertre, T. 2010, *A&A*, 510, A14+
- Linsky, J. L., Draine, B. T., Moos, H. W., Jenkins, E. B., Wood, B. E., Oliveira, C., Blair, W. P., Friedman, S. D., Gry, C., Knauth, D., Kruk, J. W., Lacour, S., Lehner, N., Redfield, S., Shull, J. M., Sonneborn, G., & Williger, G. M. 2006, *ApJ*, 647, 1106
- Louise, R. & Marcelin, M. 1983, *Ap&SS*, 91, 93
- Lubowich, D. & Pasachoff, J. M. 2010, in *IAU Symposium*, Vol. 268, *IAU Symposium*, ed. C. Charbonnel, M. Tosi, F. Primas, & C. Chiappini, 179–180
- Magrini, L., Corbelli, E., & Galli, D. 2007, *A&A*, 470, 843
- Maloney, P. R. & Putman, M. E. 2003, *ApJ*, 589, 270
- Marengo, M. 2009, *PASA*, 26, 365
- Marigo, P. & Girardi, L. 2007, *A&A*, 469, 239
- Marigo, P., Girardi, L., Bressan, A., Groenewegen, M. A. T., Silva, L., & Granato, G. L. 2008, *A&A*, 482, 883
- Marinacci, F., Binney, J., Fraternali, F., Nipoti, C., Ciotti, L., & Londrillo, P. 2010, *arXiv:1001.1835*
- Martig, M. & Bournaud, F. 2010, *ApJ*, 714, L275
- Matsuura, M., Barlow, M. J., Zijlstra, A. A., Whitelock, P. A., Cioni, M., Groenewegen, M. A. T., Volk, K., Kemper, F., Kodama, T., Lagadec, E., Meixner, M., Sloan, G. C., & Srinivasan, S. 2009, *MNRAS*, 396, 918

- Mauron, N. & Josselin, E. 2010, arXiv:1010.5369
- Miller, E. D., Bregman, J. N., & Wakker, B. P. 2009, *ApJ*, 692, 470
- Miller, G. E. & Scalo, J. M. 1979, *ApJS*, 41, 513
- Mo, H., van den Bosch, F., & White, S. 2010, *Galaxy Formation and Evolution* (Cambridge University Press)
- Murray, N. & Rahman, M. 2010, *ApJ*, 709, 424
- Noeske, K. G., Weiner, B. J., Faber, S. M., Papovich, C., Koo, D. C., Somerville, R. S., Bundy, K., Conselice, C. J., Newman, J. A., Schiminovich, D., Le Floc'h, E., Coil, A. L., Rieke, G. H., Lotz, J. M., Primack, J. R., Barmby, P., Cooper, M. C., Davis, M., Ellis, R. S., Fazio, G. G., Guhathakurta, P., Huang, J., Kassin, S. A., Martin, D. C., Phillips, A. C., Rich, R. M., Small, T. A., Willmer, C. N. A., & Wilson, G. 2007, *ApJ*, 660, L43
- Oliver, S., Frost, M., Farrah, D., Gonzalez-Solares, E., Shupe, D. L., Henriques, B., Roseboom, I., Alfonso-Luis, A., Babbedge, T. S. R., Frayer, D., Lencz, C., Lonsdale, C. J., Masci, F., Padgett, D., Polletta, M., Rowan-Robinson, M., Siana, B., Smith, H. E., Surace, J. A., & Vaccari, M. 2010, *MNRAS*, 588
- Oosterloo, T., Fraternali, F., & Sancisi, R. 2007, *AJ*, 134, 1019
- Pagel, B. E. J. 2009, *Nucleosynthesis and Chemical Evolution of Galaxies* (Cambridge University Press)
- Parriott, J. R. & Bregman, J. N. 2008, *ApJ*, 681, 1215
- Pedersen, K., Rasmussen, J., Sommer-Larsen, J., Toft, S., Benson, A. J., & Bower, R. G. 2006, *New Astronomy*, 11, 465
- Peek, J. E. G. 2009, *ApJ*, 698, 1429
- Pisano, D. J., Barnes, D. G., Gibson, B. K., Staveley-Smith, L., Freeman, K. C., & Kilborn, V. A. 2007, *ApJ*, 662, 959
- Popescu, C. C., Tuffs, R. J., Kylafis, N. D., & Madore, B. F. 2004, *A&A*, 414, 45
- Prochaska, J. X. & Wolfe, A. M. 2009, *ApJ*, 696, 1543
- Prodanović, T. & Fields, B. D. 2008, *JCAP*, 9, 3
- Prodanović, T., Steigman, G., & Fields, B. D. 2010, *MNRAS*, 406, 1108
- Putman, M. E., Henning, P., Bolatto, A., & et al. 2009a, in *ArXiv Astrophysics e-prints*, Vol. 2010, astro2010 white paper (arXiv/0902.4717), 241–+
- Putman, M. E., Peek, J. E. G., & Heitsch, F. 2009b, arXiv:0907.1023
- Putman, M. E., Peek, J. E. G., Muratov, A., Gnedin, O. Y., Hsu, W., Douglas, K. A., Heiles, C., Stanimirovic, S., Korpela, E. J., & Gibson, S. J. 2009c, *ApJ*, 703, 1486
- Raiteri, C. M., Villata, M., & Navarro, J. F. 1996, *A&A*, 315, 105
- Rand, R. J. & Benjamin, R. A. 2008, *ApJ*, 676, 991
- Rasmussen, J., Sommer-Larsen, J., Pedersen, K., Toft, S., Benson, A., Bower, R. G., & Grove, L. F. 2009, *ApJ*, 697, 79
- Rasmussen, J., Sommer-Larsen, J., Pedersen, K., Toft, S., Benson, A., Bower, R. G., & Olsen, L. F. 2006, *ArXiv Astrophysics e-prints*
- Rhode, K. L., Windschitl, J. L., & Young, M. D. 2010, *AJ*, 140, 430
- Roberts, M. S. 1963, *ARA&A*, 1, 149
- Robitaille, T. P. & Whitney, B. A. 2010, *ApJ*, 710, L11
- Rocha-Pinto, H. J., Scalo, J., Maciel, W. J., & Flynn, C. 2000, *A&A*, 358, 869
- Rodighiero, G., Cimatti, A., Gruppioni, C., Popesso, P., Andreani, P., Altieri, B., Aussel, H., Berta, S., Bongiovanni, A., Brisbin, D., Cava, A., Cepa, J., Daddi, E., Dominguez-Sanchez, H., Elbaz, D., Fontana, A., Forster Schreiber, N., Franceschini, A., Genzel, R., Grazian, A., Lutz, D., Magdis, G., Magliocchetti, M., Magnelli, B., Maiolino, R., Mancini, C., Nordon, R., Perez Garcia, A. M., Poglitsch, A., Santini, P., Sanchez-Portal, M., Pozzi, F., Riguccini, L., Saintonge, A., Shao, L., Sturm, E., Tacconi, L., Valchanov, I., Wetzstein, M., & Wierprecht, E. 2010, arXiv:1005.1089
- Rudd, D. H., Zentner, A. R., & Kravtsov, A. V. 2008, *ApJ*, 672, 19
- Saitoh, T. R., Daisaka, H., Kokubo, E., Makino, J., Okamoto, T., Tomisaka, K., Wada, K., & Yoshida, N. 2008, *PASJ*, 60, 667
- Salim, S., Rich, R. M., Charlot, S., Brinchmann, J., Johnson, B. D., Schiminovich, D., Seibert, M., Mallery, R., Heckman, T. M., Forster, K., Friedman, P. G., Martin, D. C., Morrissey, P., Neff, S. G., Small, T., Wyder, T. K., Bianchi, L., Donas, J., Lee, Y., Madore, B. F., Milliard, B., Szalay, A. S., Welsh, B. Y., & Yi, S. K. 2007, *ApJS*, 173, 267
- Salpeter, E. E. 1955, *ApJ*, 121, 161
- Sancisi, R., Fraternali, F., Oosterloo, T., & van der Hulst, T. 2008, *A&A Rev.*, 15, 189
- Sandage, A. 1986, *A&A*, 161, 89
- Scalo, J. 1998, in *Astronomical Society of the Pacific Conference Series*, Vol. 142, *The Stellar Initial Mass Function* (38th Herstmonceux Conference), ed. G. Gilmore & D. Howell, 201–+
- Scalo, J. M. 1986, *Fundamentals of Cosmic Physics*, 11, 1
- Schaye, J., Dalla Vecchia, C., Booth, C. M., Wiersma, R. P. C., Theuns, T., Haas, M. R., Bertone, S., Duffy, A. R., McCarthy, I. G., & van de Voort, F. 2010, *MNRAS*, 402, 1536
- Sembach, K. R., Wakker, B. P., Savage, B. D., Richter, P., Meade, M., Shull, J. M., Jenkins, E. B., Sonneborn, G., & Moos, H. W. 2003, *ApJS*, 146, 165
- Sonneborn, G., Tripp, T. M., Ferlet, R., Jenkins, E. B., Sofia, U. J., Vidal-Madjar, A., & Woźniak, P. R. 2000, *ApJ*, 545, 277
- Srinivasan, S., Meixner, M., Leitherer, C., Vihj, U., Volk, K., Blum, R. D., Babler, B. L., Block, M., Bracker, S., Cohen, M., Engelbracht, C. W., For, B., Gordon, K. D., Harris, J., Hora, J. L., Indebetouw, R., Markwick-Kemper, F., Meade, M., Misselt, K. A., Sewilo, M., & Whitney, B. 2009, *AJ*, 137, 4810
- Stanghellini, L., Magrini, L., Villaver, E., & Galli, D. 2010, *A&A in press* (arXiv/1006.4076), 521, A3+
- Stark, D. P., Ellis, R. S., Bunker, A., Bundy, K., Targett, T., Benson, A., & Lacy, M. 2009, *ApJ*, 697, 1493
- Steigman, G., Romano, D., & Tosi, M. 2007, *MNRAS*, 378, 576
- Stinson, G., Seth, A., Katz, N., Wadsley, J., Governato, F., & Quinn, T. 2006, *MNRAS*, 373, 1074
- Tassis, K., Kravtsov, A. V., & Gnedin, N. Y. 2008, *ApJ*, 672, 888
- Thilker, D. A., Braun, R., Walterbos, R. A. M., Corbelli, E., Lockman, F. J., Murphy, E., & Maddalena, R. 2004, *ApJ*, 601, L39
- Tinsley, B. M. 1980, *Fundamentals of Cosmic Physics*, 5, 287
- van Loon, J. T., Stanimirović, S., Putman, M. E., Peek, J. E. G., Gibson, S. J., Douglas, K. A., & Korpela, E. J. 2009, *MNRAS*, 396, 1096
- Vassiliadis, E. & Wood, P. R. 1993, *ApJ*, 413, 641
- Wakker, B. P., York, D. G., Howk, J. C., Barentine, J. C., Wilhelm, R., Peletier, R. F., van Woerden, H., Beers, T. C., Ivezić, Ž., Richter, P., & Schwarz, U. J. 2007, *ApJ*, 670, L113
- Wakker, B. P., York, D. G., Wilhelm, R., Barentine, J. C., Richter, P., Beers, T. C., Ivezić, Ž., & Howk, J. C. 2008, *ApJ*, 672, 298
- Walterbos, R. A. M. & Braun, R. 1994, *ApJ*, 431, 156
- Welch, G. A., Sage, L. J., & Young, L. M. 2010, *ApJ in press* (arXiv/1009.5259)
- Wilkins, S. M., Hopkins, A. M., Trentham, N., & Tojeiro, R. 2008, *MNRAS*, 391, 363
- Williams, B. F. 2003, *AJ*, 126, 1312
- Wood, B. E., Linsky, J. L., Hébrard, G., Williger, G. M., Moos, H. W., & Blair, W. P. 2004, *ApJ*, 609, 838
- Woodsley, S. E. & Weaver, T. A. 1995, *ApJS*, 101, 181
- Zheng, X. Z., Bell, E. F., Papovich, C., Wolf, C., Meisenheimer, K., Rix, H., Rieke, G. H., & Somerville, R. 2007, *ApJ*, 661, L41